ACS OMEGA

http://pubs.acs.org/journal/acsodf

Article

Stress–Strain and Stress-Relaxation Behaviors of Solution-Coated Layers Composed of Block Copolymers Mixed with Tackifiers

Takahiro Doi, Hideaki Takagi, Nobutaka Shimizu, Noriyuki Igarashi, and Shinichi Sakurai*

Cite This: *ACS Omega* 2021, 6, 17299–17313

Read Online

ACCESS | Metrics & More | Article Recommendations | Supporting Information

ABSTRACT: The relationship between the mechanical properties and the structure of block copolymers mixed with tackifiers whose relative solubility to the respective components of block copolymers differs was examined. Coated layers were prepared by solution coating using a block copolymer composed of polystyrene (PS) and polyisoprene (PI), which forms spherical microdomains of PS in the PI matrix, mixed with three types of tackifiers: aliphatic (C5) resin, aliphatic–aromatic (C5–C9) resin, and rosin ester (RE) resin. Furthermore, the correlation between the changes in the nanostructure and mechanical properties including the stress-relaxation behaviors was clarified by two-dimensional small-angle X-ray scattering measurement. The amount of the PI-bridge conformation in the case of C5 resin is the lowest, resulting in the lowest stress. On the contrary, the largest amount of RE resin was solubilized in the PS phase so that it can be considered that pulling out of the PS chains took place easily. We were able to explain the stress-relaxation behavior by fitting with the three-component exponent functions. The triple exponential decay functions indicate the hierarchy of the structures that are the origins of the "fast mode" relating to the local relaxation due to the rotation of the repeating unit of polymer chains; the "intermediate mode" of the disentanglement of the mid-PI chains; and the "slow mode" relating to, in this particular case, pulling out of the PS chains from the PS sphere.

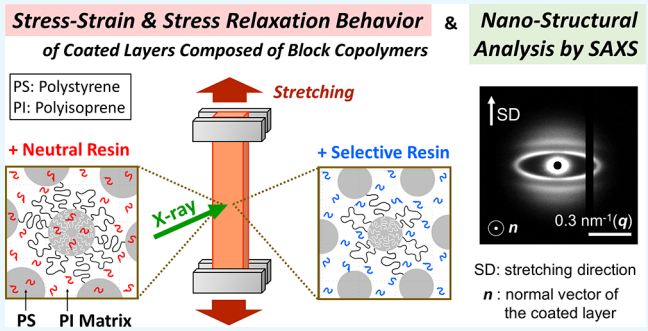

1. INTRODUCTION

Tuning mechanical properties of block copolymers is an important issue to develop new block copolymer materials with tailored properties. Needless to say, the controlling morphologies of microdomains is important for the control of the mechanical properties. The blending of homopolymers,[1−5] other block copolymers,[6,7] or plasticizer molecules[8] with block copolymers has been examined as a strategy to control the morphology through altering the total composition of A and B phases. It should be noted that this strategy works well for the morphology control in case of the wet brush under the term of "quasi-one component system", while it does not completely work in case of the dry-brush condition. Here, the wet-brush condition indicates the situation that the added polymer chains (or the plasticizer molecules favoring mixing into one component or both components) can be homogeneously mixed with the block chains in the microdomain space,[2,9−18] while the dry-brush condition specifies the situation that the added polymer chains are localized in the microdomain space even though the added components are chemically the same as those of the microdomain.[2,10,19] Note that the addition of plasticizer (or tackifier) molecules can always meet the wet-brush condition. In line with the wet-brush condition, let us consider the case when the B-component polymer chains or B-component favorable plasticizer (or tackifier) molecules are being added into the B matrix phase that embeds A-spheres of ABA-type triblock copolymers as a typical example. Note here that such ABA-type triblock copolymers can be utilized as a thermoplastic elastomer when the A-component is glassy (hard) and the B-component is rubbery (soft). Although further reducing the total A fraction from the above-stated case with the A-spherical microdomains suggests seemingly nothing of interest because of no further morphological transition expected, even for this case, it was found in our previous study that controlling the size of the A-spheres was possible. Actually, it was found that the A-spheres became smaller upon the addition of the B-component favorable tackifier molecules.[20] For this particular case, it is also expected that the mechanical properties change (reduction of the tensile modulus/acceleration of the stress relaxation) because the fraction of the loop conformation of the B-block chains is increased while the fraction of their bridge conformation is complementarily decreased. Here, it should be noted that when the hard end-block chains (A-block in the ABA-type triblock copolymer) are

Received: March 14, 2021
Accepted: May 28, 2021
Published: July 1, 2021

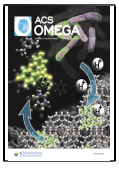

Table 1. Molecular Characteristics of Block Copolymers and Tackifiers

					PS content[a]			T_g (°C)[b]	
		code	M_w[c]	M_w/M_n[d]	(wt %)	(vol %)	SI content (wt %)	PI[e]	PS[f]
block copolymer		SIS[g]	207,000	1.03	16	14			
		SI[h]	101,000	1.04	16	14			
		SIS/SI			16	14	56	−61.2	86.2
	code		classification		M_w[c]	M_w/M_n[d]	T_g (°C)[b]	remark	
tackifier	C5		aliphatic resin		1180	1.92	47.1	selective solvent (solubilized in PI)	
	C5−C9		aliphatic−aromatic resin		1120	2.37	42.7	intermediate character between C5 and RE	
	RE		rosin ester resin		750	1.05	57.7	neutral solvent (solubilized in PI and PS)	

Reprinted in part with permission from ref 20. Copyright 2020/ACS Publications. [a]PS total content in the blend specimen, expressed as weight content (wt %). The volume content (vol %) is converted from the wt % value by using the mass density values for polystyrene (=1.04−1.065 g/cm^3)[29] and polyisoprene (=0.913 g/cm^3).[30] [b]T_g : glass transition temperature [determined by differential scanning calorimetry (DSC)]. [c]M_w : weight-averaged molecular weight [determined by gel permeation chromatography (GPC), polystyrene equivalent]. [d]M_w/M_n: polydispersity index of molecular weights, where M_n is the number-averaged molecular weight (determined by GPC). [e]PI: polyisoprene. [f]PS: polystyrene. [g]SIS: polystyrene-*block*-polyisoprene-*block*-polystyrene triblock copolymer. [h]SI: polystyrene-*block*-polyisoprene diblock copolymer.

separately incorporated in the adjacent hard spherical microdomains, the conformation of the soft mid-block chains (B-block in the ABA-type triblock copolymer) is referred to as the bridge conformation. On the other hand, when the hard end-block chains are incorporated in the identical hard spherical microdomains, the conformation of the soft mid-block chains is referred to as the loop conformation.

To prove our speculation, the current study is aimed at understanding the effects of the solubility difference of tackifiers on the mechanical properties and those on the stress-relaxation behaviors in the materials of SIS/SI-tackifier with various types where the tackifier solubility to PS (polystyrene) and that to PI (polyisoprene) differ (SIS: polystyrene-*block*-polyisoprene-*block*-polystyrene triblock copolymer/SI: polystyrene-*block*-polyisoprene diblock copolymer). Here, it is important to correlate such mechanical properties (especially the stress-relaxation behaviors) with the deformation of the hard glassy spherical microdomains. It has been recently reported by Tomita et al.[21,22] that the glassy spherical microdomains suffered serious deformation (shape change from sphere to spheroid with the extent of up to 20% elongation of the long radius) upon the uniaxial stretching even at a temperature that is far below the glass transition temperature (T_g) of the hard segment, which may be the crucial reason for the macroscopic breakdown of the film specimen used for the stress-relaxation measurements. They conducted the 2D-SAXS measurements using the synchrotron X-ray to detect the deformation of the PS spherical microdomains in a stretched SEBS [polystyrene-*block*-poly(ethylene-*co*-butylene)-*block*-polystyrene] triblock copolymer film by focusing on the shifts of the particle scattering peak toward lower and higher q regions in directions parallel and perpendicular to the stretching direction (SD), respectively, where q denotes the magnitude of the scattering vector. Note here that the particle scattering means the scattering component being ascribed to the particle interference, which is different from the lattice factor due to the interparticle interference (due to the ordering regularity of the ordered particles). In the current study, we will also focus on the deformation of the PS sphere in the neat SIS/SI block copolymer specimen.

A pressure-sensitive adhesive utilizes an ABA-type triblock copolymer as a base polymer.[23,24] The hard A phase contributes cohesive property, and the soft B phase does initial adhesion to the adherend (so-called tackiness). To sufficiently meet these requirements, diblock copolymers are usually blended with triblock copolymers for the purpose of softening,[25] and the blends are compounded with tackifiers[20,26−28] to further impart functionality such as tackiness, adhesiveness, and fixability to an adherend. We quantitatively analyzed by SAXS measurement the effects of solubility difference of the tackifier to the respective components of styrenic block copolymers on microphase-separated structures.[20] For this purpose, coated layers were prepared by the solution coating method using a blend of the SIS triblock copolymer and SI diblock copolymer, which forms spherical microdomains of PS in the PI matrix, mixed with three types of tackifiers: aliphatic (C5) resin, aliphatic−aromatic (C5−C9) resin, and rosin ester (RE) resin (the SIS/SI-tackifier specimens). The RE resin is considered to be solubilized homogeneously into both of PS and PI, while the C5 resin is only solubilized in the PI matrix phase due to its immiscibility with PS. The pressure-sensitive adhesive tape has a multilayer structure with an adhesive layer, a substrate layer, and a release layer. Among them, the adhesive layer is the layer that contributes most to the adhesive performance and has a wide variety of designs. In particular, the type of tackifier added to the block copolymer contributes to the adhesive performance and is very important in the adhesive compound design. Furthermore, to understand adhesive properties, it is important to evaluate the mechanical properties such as stress−strain and stress-relaxation behaviors for the pressure-sensitive adhesive layer. This is because the adhesive layer is subjected to the deformation when the adhesive tape is peeled off from the adherend surface in case of cleaning after use. The shear deformation behavior is also important when considering the long-term durability of the adhesive layer used to fix a poster on a wall against the vertical load due to the gravity or used to pack a shipping box against the reversing force.

In the current study, we revealed the effects of solubility difference of the tackifier to the respective components of block copolymers on mechanical properties for the same SIS/SI-tackifier specimens used in our previous study.[20] For this purpose, the stress−strain, shear force, and stress-relaxation measurements at various stretching ratios were performed. From the stress−strain measurements, the changes in the ratios of bridge/loop conformation of the mid-PI block chains in the SIS triblock copolymer for the SIS/SI-tackifier specimens are quantitatively discussed. As for the stress relaxation, the temporal change of the stress is explained with a complex

https://doi.org/10.1021/acsomega.1c01367
ACS Omega 2021, 6, 17299−17313

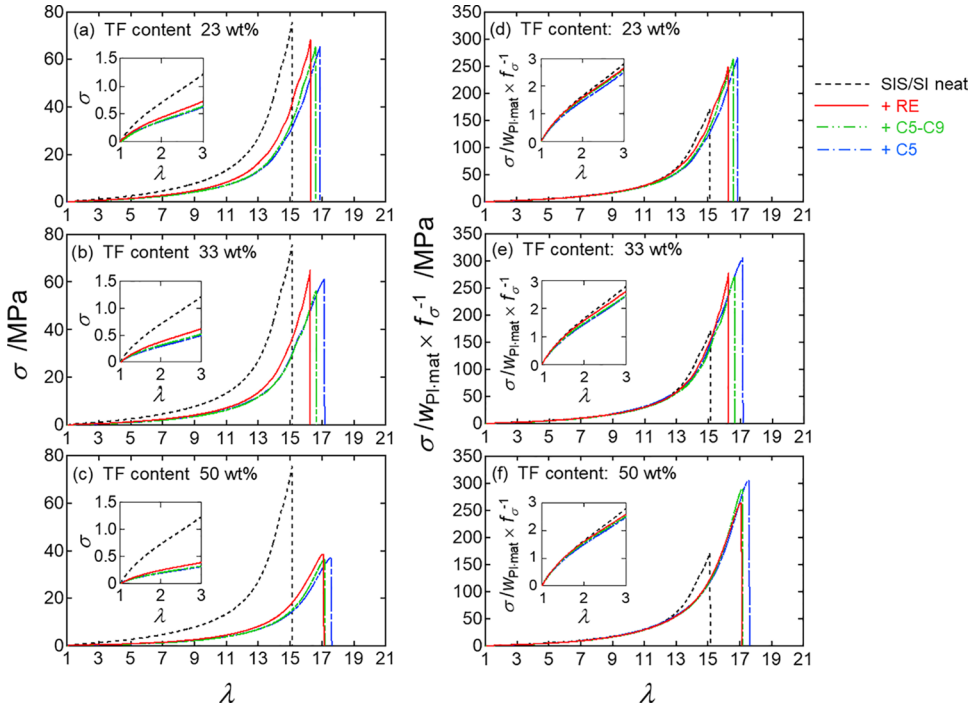

Figure 1. (a–c) True S–S curves (σ vs λ curves) for the SIS/SI-tackifier specimens with various types of tackifiers, including the result for the neat SIS/SI specimen at room temperature. The expanded views to focus on the behaviors at low stretching ratio of all specimens are shown together in the insets. (d–f) Normalized S–S curves ($\sigma/w_{\text{PI·mat}} \times f_\sigma^{-1}$ vs λ curves). The tackifier contents are (a, d) 23, (b, e) 33, and (c, f) 50 wt %. Here, $w_{\text{PI·mat}}$ indicates the weight fraction of PI block chains of the SIS triblock in the matrix of the SIS/SI-tackifier specimen, and f_σ designates a shift factor to attain almost complete overlaps (master curve) of the S–S curves ($\sigma/w_{\text{PI·mat}}$ vs λ curves) with the SIS/SI neat behavior in the range of $1 \leq \lambda \leq 12$. Refer to Figure S1 in the Supporting Information for the $\sigma/w_{\text{PI·mat}} - \lambda$ curves.

mathematical function. Furthermore, understanding of the structural change during stretching is crucial for a better understanding of the structure–mechanical property relationship. We rigorously intended to understand the mechanical properties (the stress–strain and stress-relaxation behaviors) of the SIS/SI-tackifier specimens in terms of the structural change upon the stretching of the specimens by conducting 2D-SAXS measurements at room temperature.

2. RESULTS AND DISCUSSION

2.1. Stress–Strain Behavior. The molecular characteristics of block copolymers and tackifiers are listed in Table 1. Figure 1a–c shows the true stress–stretching ratio (S–S) curves (σ vs λ curves, where λ denotes the true stretching ratio) for the SIS/SI-tackifier specimens with various types of tackifiers, including the result for the neat SIS/SI specimen at room temperature. The tackifier contents are (a) 23, (b) 33, and (c) 50 wt %. The expanded views to focus on the behaviors at low stretching ratio of all specimens are shown together in the insets. When λ was less than 12, the stress increased gradually, but for the successive stage ($\lambda \geq 12$), the stress increased drastically, irrespective of the specimens. It was found that the S–S curves of all SIS/SI-tackifier specimens had lower overall stress and higher elongation at break than those of the SIS/SI neat specimen. However, it is obvious that the order in the level of degree of overall stress reduction and increase of elongation at break was C5 > C5–C9 > RE. Also, the overall stress decreased with an increase in the tackifier content, with the SIS/SI-C5 resin specimens being the lowest.

The stress reduction is considered to be ascribed to a decrease in the fraction of the bridge conformation of the mid-PI block chains in the SIS triblock copolymer in the matrix (PI·mat) because the loop conformation of the mid-PI chains cannot impart the stress in the slightly stretched specimen. To confirm this conjecture, the stress is normalized by the fraction of the PI·mat ($w_{\text{PI·mat}}$) because the stress is proportional to the number of the stretched PI chains, which is especially correct in the initial stage of stretching. Figure S1 (in the Supporting Information) shows the S–S curves normalized by $w_{\text{PI·mat}}$ ($\sigma/w_{\text{PI·mat}} - \lambda$ curves) for the SIS/SI-tackifier specimens with various types of tackifiers, including the result for the neat SIS/SI specimen. Nevertheless, the normalized S–S curves did not merge together. Rather, they were more decreased with an increase in the tackifier content and also decreased in the order of RE < C5–C9 < C5. The reduction of the normalized stress ($\sigma/w_{\text{PI·mat}}$) of the SIS/SI-tackifier specimens compared to that of the SIS/SI neat specimen implies the decrease in the fraction of the bridge conformation. Based on the idea that the reduction in the normalized stress ($\sigma/w_{\text{PI·mat}}$) is ascribed to the decrease in the fraction of the bridge conformation, we tried to evaluate the reduction factor (f_σ) from the normalized S–S curve. Figure 1d–f shows the master curves of $\sigma/w_{\text{PI·mat}}$ with the shift factor (f_σ^{-1}) to attain almost complete overlaps of the S–S curves in the range of $1 \leq \lambda \leq 12$. Note that these overlap operations were conducted by the vertical shift with the shift factor (f_σ^{-1}) for the plot of the log ($\sigma/w_{\text{PI·mat}}$) vs strain, shown in Figure S2 in the Supporting Information. While the completeness of the master curve in the range of $1 \leq \lambda \leq 12$, the $\sigma/w_{\text{PI·mat}}$ curves deviated much from that for the SIS/SI neat specimen in the range of $\lambda > 12$. This negative deviation may be due to a decrease in the physical entanglement of the PI chains due to the presence of the tackifier molecules, which contribute to the prolonged elongation at break with the order of C5 > C5–C9 > RE for the 33 wt % tackifier content. It is

https://doi.org/10.1021/acsomega.1c01367
ACS Omega 2021, 6, 17299–17313

interesting to note that this tendency diminishes as the tackifier content increases, and eventually, the three curves completely overlap in the case of 50 wt % tackifier content with a slight difference in the ultimate elongation (improved extensibility due to the solubilization of the tackifier molecules).

The Young's modulus (E), the normalized Young's modulus ($E/w_{PI\cdot mat}$), and the conversion factor for $E/w_{PI\cdot mat}$ (f_E) were also evaluated from the S−S curves (σ vs λ curves and $\sigma/w_{PI\cdot mat}$ vs λ curves) and plotted as a function of the tackifier content in Figure 2. Here, the E was obtained from the primary

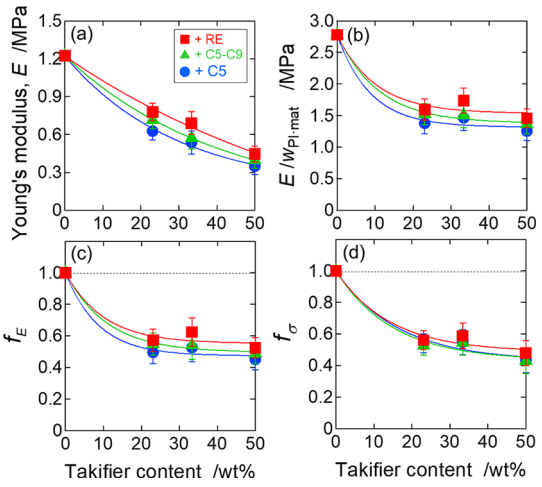

Figure 2. Plots of (a) Young's modulus (E), (b) normalized Young's modulus ($E/w_{PI\cdot mat}$), (c) the conversion factor for $E/w_{PI\cdot mat}$ (f_E), and (d) the shift factor for the S−S curves (f_σ) as a function of the tackifier content for the SIS/SI-tackifier specimens. Note that f_E was evaluated as $f_E = (E/w_{PI\cdot mat})_{TF}/(E/w_{PI\cdot mat})_{neat}$, where the suffix "TF" indicates the specimens with tackifier and "neat" stands for the neat SIS/SI specimen.

differential coefficient of σ with respect to λ ($d\sigma/d\lambda$). It is found that the $E/w_{PI\cdot mat}$ decreased with the tackifier content, as well as the E. As mentioned above, the stress in the initial stage of stretching is proportional to the number of the PI chains with the bridge conformation. Therefore, the still decreasing tendency in Figure 2b with the increase in the tackifier content after the normalization by $w_{PI\cdot mat}$ suggests the reduction in the fraction of the bridge conformation. Watanabe et al. experimentally estimated the bridge/loop faction of $(SI)_2$ triblock copolymers using the dielectric relaxation measurements, where the dielectric data exclusively detected the fluctuation of the midpoint of the dipole-inverted PI block chains having either bridge or loop conformation.[31−34] As a result, it was found that the addition of a PI-selective solvent, n-tetradecane, to the SIS (SIIS) triblock copolymer increased the PI-loop fraction.[32] This increase of the PI-loop fraction was attributed to the stretching and destabilization of the bridge configuration on dilution. Furthermore, for the triblock/diblock blend, the dielectric data of SIS triblock copolymer hardly change on blending with the SI diblock copolymer.[33] Within the hypothesis, the blending is equivalent to an addition of loops to the SIS system, and the re-equilibration of SIS conformation can keep the same bridge/(loop + tail) ratio to give the same dielectric data. Note that the SI diblock copolymer had noninverted type-A dipoles in the PI block, while the SIIS copolymer, a head-to-head coupled dimer of the SI diblock copolymer, had once-inverted dipoles in the PI block chains. Such experimental results are very reliable and are considered to be universal in SIS-based materials so that we can consider a similar situation for our specimens where the elements that plasticize the respective components of block copolymers (PI and PS phases) are tackifiers whose solubility in the respective components differs (as they are considered to be selective or neutral solvents). Note that the f_E shown in Figure 2c was evaluated as $f_E = (E/w_{PI\cdot mat})_{TF}/(E/w_{PI\cdot mat})_{neat}$, where the suffix "TF" indicates the specimens with tackifier and "neat" stands for the neat SIS/SI specimen. Note also that the decreasing tendency of f_E as a function of the tackifier content is similar to that of f_σ. This is reasonable because f_E reflects the S−S behavior in the limit of $\lambda \to 1$, while f_σ does that in the wide range with $1 \le \lambda \le 12$. Those decreasing tendencies clearly indicate that the bridge fraction rapidly decreases within 20 wt % of the tackifier added in the SIS/SI neat specimens, while the further amounts of the tackifier added do not so effectively decrease the bridge fraction. Thus, this nonlinear effect of the addition of the tackifier is noteworthy.

It is also interesting to note that the effect of the tackifier on the reduction of the bridge fraction depends slightly on the type of the tackifier, as it is in the order of RE < C5−C9 < C5. To understand this tendency, the structural model reported in our previous publication[20] is considered. Figure 3 illustrates the effects of solubilization of tackifiers into the PI matrix phase on the fraction of the bridge conformation of the mid-PI block chains of the SIS triblock copolymer. Note that the case of the SIS triblock copolymer neat is considered for simplicity as shown in panel (a). Here, it is reasonably assumed that the fraction of the bridge conformation is identical to that of the loop conformation for the bulk (without any solubilized tackifier molecules) from the literature knowledge.[32,34] In the case of the RE resin, this tackifier can be equally solubilized in both the PS and PI phases so that the tackifier content in the PI matrix phase is identical to the net tackifier content [panel (b)]. On the other hand, in the case of the C5 resin, this tackifier can be only solubilized in the PI matrix phase because of its character as a selective solvent. This situation is illustrated in panel (c). Therefore, the tackifier content in the PI matrix phase becomes larger than the net tackifier content. In other words, the $w_{PI\cdot mat}$ is higher in the case of the RE resin than that in the case of the C5 resin. Therefore, the S−S curves should be normalized by $w_{PI\cdot mat}$ for the appropriate comparison. As shown in Figure S1 in the Supporting Information, it is clearly found that the specimens blended with the tackifier exhibited lower stress even after the normalization. This indicates the lowering of the fraction of the bridge conformation. As a matter of fact, the values of f_σ and f_E (which can be the index of the fraction of the bridge conformation) in Figure 2c,d decrease with the tackifier content. Furthermore, f_σ and f_E were found to be lower in the case of the C5 resin as compared to the RE resin. Therefore, it is concluded that the amount of the bridge conformation in the case of the C5 resin is lesser than that in the case of the RE resin. This situation is illustrated in panel (c). Note also here that smaller PS spheres are illustrated in panel (b) as compared to the ones in panel (a) and that much smaller PS spheres are illustrated in panel (c). These facts have been revealed by the structural analyses using the SAXS technique, and such strange change (reduction of the sphere size upon addition of tackifiers) was explained in detail in our previous publication.[20]

https://doi.org/10.1021/acsomega.1c01367
ACS Omega 2021, 6, 17299−17313

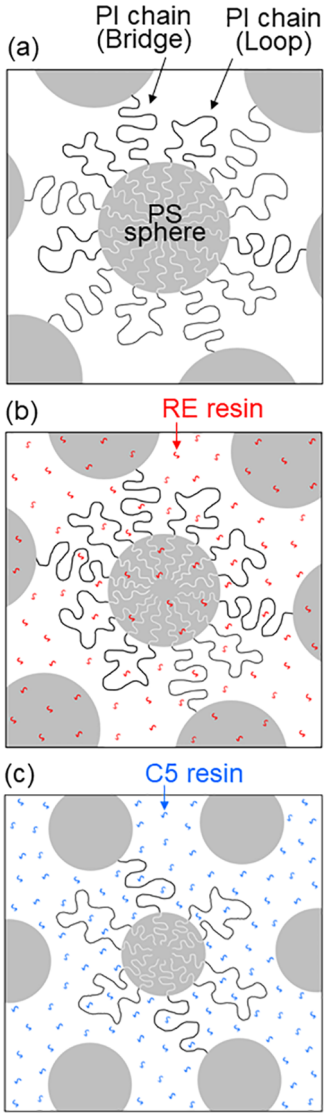

Figure 3. Schematic illustrations showing the effects of solubilization of tackifiers into the PI matrix phase on the fraction of the bridge conformation of the mid-PI block chains of the SIS triblock copolymer. Note that the case of the SIS triblock copolymer neat is considered for simplicity as shown in panel (a). In the case of the RE resin, this tackifier can be equally solubilized in both the PS and PI phases so that the tackifier content in the PI matrix phase is identical to the net tackifier content [panel (b)]. On the other hand, in the case of the C5 resin, this tackifier can only be solubilized in the PI matrix phase because of its character as a selective solvent. Based on the results plotted in Figures 2c,d, it is concluded that the amount of the bridge conformation in the case of the C5 resin is lesser than that in the case of the RE resin. This situation is illustrated in panel (c). Note also here that smaller PS spheres are illustrated in panel (b) as compared to the ones in the panel (a) and that much smaller PS spheres are illustrated in panel (c). These facts have been revealed by the structural analyses using the SAXS technique and were explained in detail in our previous publication.[20] Reprinted in part with permission from ref 20. Copyright 2020/ACS Publications.

2.2. Nanostructural Analysis of the Stretched Specimen. To clarify the correlation between the changes in the nanostructure and mechanical properties, we conducted an analysis of the structural changes upon uniaxial stretching by 2D-SAXS measurements. It was found from Figure S3 in the Supporting Information that the through-view 2D-SAXS pattern of the initial state before stretching (λ = 1) exhibiting a round shape[20] changed into an elliptic shape. Note that the q value of the first-order peak is ascribed to the {110} plane of the body-centered-cubic (bcc) lattice. Figure 4 shows the 1D-SAXS profiles for the SIS/SI neat specimen stretched at (a) λ = 2 and (b) λ = 13. Those profiles were obtained from the through-view 2D-SAXS patterns (shown in Figure S3 in the Supporting Information) by conducting the sector average. Note that the sector average was conducted with the azimuthal angle range of $\mu = 90° \pm 1°$ and $\mu = 0° \pm 1°$ for the $\boldsymbol{q}$ direction parallel to SD ($\boldsymbol{q}$ // SD) and perpendicular to SD ($\boldsymbol{q} \perp$ SD), respectively. The definition of μ is given in Figure S3a1. Note here that the black symbols show the profiles obtained just after reaching the stretching state, while the red symbols show the one measured at 10 min elapsed. The blue curves indicate the model particle scattering profile calculated by assuming Gaussian distribution for the sphere radius R (see the Supporting Information) to represent the particle scattering peak in the experimentally obtained 1D-SAXS profiles. Panel (c) shows changes in the average radius (R) of the PS spherical microdomain with λ in the direction parallel and perpendicular to SD for the SIS/SI neat specimen, as schematically illustrated in this panel. Here, the broken line indicates the value of R (R_0) for the unstretched specimen (the R is the same in both of the directions parallel and perpendicular to SD). Note also that the solid and dotted−broken curves indicate the deformation behavior with $R_{//SD} = R_0 \cdot \lambda$ and $R_{\perp SD} = R_0 / \sqrt{\lambda}$ by assuming affine deformation with a constant volume of the PS sphere during the stretching. Here, $R_{//SD}$ and $R_{\perp SD}$ denote the R in the direction parallel and perpendicular to SD, respectively.

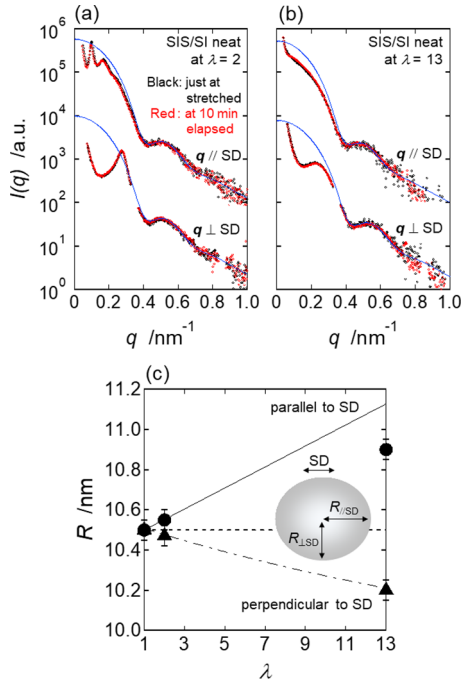

Figure 4. 1D-SAXS profiles for the SIS/SI neat specimen stretched at (a) λ = 2 and (b) λ = 13. Those profiles were obtained from the through-view 2D-SAXS patterns (shown in Figure S3 in the Supporting Information) by conducting the sector average. Note that the sector average was conducted with the azimuthal angle range of $\mu = 90° \pm 1°$ and $\mu = 0° \pm 1°$ for the $\boldsymbol{q}$ direction parallel to SD ($\boldsymbol{q}$ // SD) and perpendicular to SD ($\boldsymbol{q} \perp$ SD), respectively. The definition of μ is given in Figure S3a1. Note here that the black symbols show the profiles obtained just after reaching the stretched state, while the red symbols show the one obtained at 10 min elapsed. The blue curves indicate the model particle scattering profile calculated by assuming Gaussian distribution for the sphere radius R (see the Supporting Information) to represent the particle scattering peak in the experimentally obtained 1D-SAXS profiles. Panel (c) shows changes in the average radius (R) of the PS spherical microdomain with λ in the direction parallel and perpendicular to SD for the SIS/SI neat specimen, as schematically illustrated in this panel. Here, the broken line indicates the value of R (R_0) for the unstretched specimen (the R is the same in both of the directions parallel and perpendicular to SD). Note also that the solid and dotted−broken curves indicate the deformation behavior with $R_{//SD} = R_0 \cdot \lambda$ and $R_{\perp SD} = R_0 / \sqrt{\lambda}$ by assuming affine deformation with a constant volume of the PS sphere during the stretching. Here, $R_{//SD}$ and $R_{\perp SD}$ denote the R in the direction parallel and perpendicular to SD, respectively.

https://doi.org/10.1021/acsomega.1c01367
ACS Omega 2021, 6, 17299−17313

elapsed from the onset of the stretched state at a given λ. When the SIS/SI neat specimen was stretched, the q value of the first-order peak in $\boldsymbol{q}$ // SD shifted toward the lower q region, while in $\boldsymbol{q} \perp$ SD, the q value of the first-order peak shifted toward the higher q region, because of an increase in the d spacing in the direction parallel to SD and a decrease in the d spacing in the direction perpendicular to SD. Furthermore, similar shifts in the q value of the broad peaks (the particle scattering peak, q_m) were observed in the range of $0.4 < q < 0.7$. The q value of the particle scattering peaks for the specimen stretched at $\lambda = 13$ shifted toward lower and higher regions in $\boldsymbol{q}$ // SD and $\boldsymbol{q} \perp$ SD, respectively. This result implies the deformation of the glassy PS spheres. Actually, the deformation of the glassy PS spheres (stretched at $\lambda = 4$) has been reported by Tomita et al. for polystyrene-*block*-poly(ethylene-*co*-butylene)-*block*-polystyrene (SEBS) specimens with a relatively low-molecular-weight PS block chain.[21,22] Note that the average radius of PS spheres (R) can be estimated through the calculation of the model particle scattering profile by assuming Gaussian distribution for the sphere radius R (see the Supporting Information). Panel (c) shows changes in thus-evaluated average radius (R) of the PS spherical microdomain with λ in the direction parallel and perpendicular to SD for the SIS/SI neat specimen, as schematically illustrated in this panel. Here, the broken line indicates the value of R (R_0) for the unstretched specimen (the R is the same in both of the directions parallel and perpendicular to SD). Note also that the solid and dotted−broken curves indicate the deformation behavior with $R_{//SD} = R_0 \cdot \lambda$ and $R_{\perp SD} = R_0 / \sqrt{\lambda}$ by assuming the affine deformation with a constant volume of the PS sphere during the stretching. Here, $R_{//SD}$ and $R_{\perp SD}$ denote the R in the direction parallel and perpendicular to SD, respectively. It is noteworthy that the experimental result of $R_{//SD}$ at $\lambda = 13$ is much smaller than the expected one (the solid line), whereas the other experimental results (data points) follow the anticipation. This fact implies the following two aspects: (1) the hard PS spheres could not be deformed so highly, and (2) they were broken at around $\lambda \cong 9$. Note that we reported a slightly larger value of $R = 11.6$ nm in our previous paper for the SIS/SI neat specimen before stretching.[20] This is simply because of the difference in the evaluation method where the relationship with $q_m \cdot R = 5.765$ was utilized in our previous paper and R was evaluated from the peak position (q_m) of the particle scattering for the spherical particle.[35] In addition, for the SIS/SI neat specimen, the fact that the 1D-SAXS profiles just after reaching the stretched state and at 10 min elapsed were almost identical indicates that there was no structural change during 10 min at the stretched state at $\lambda = 2$ and 13.

We investigated the structural changes upon uniaxial stretching for the SIS/SI-tackifier (with the three types of tackifier) specimens. First of all, the 1D-SAXS results of the case of lower stretching ($\lambda = 2$) for the specimens with a relatively lower amount of tackifier (33 wt %) are examined in Figure 5. Those profiles were obtained from the through-view 2D-SAXS patterns (shown in Figure S4 in the Supporting Information) by conducting the sector average. Note here that the black symbols show the profiles obtained just after reaching the stretched state, while the red symbols show the one obtained at 10 min elapsed. In contrast to the results of the SIS/SI neat specimen, the scattering intensity of the first-order peak at 10 min elapsed was reduced compared to that just after reaching the stretched state, irrespective of the types of tackifier. Furthermore, at 10 min elapsed, the first-order peak

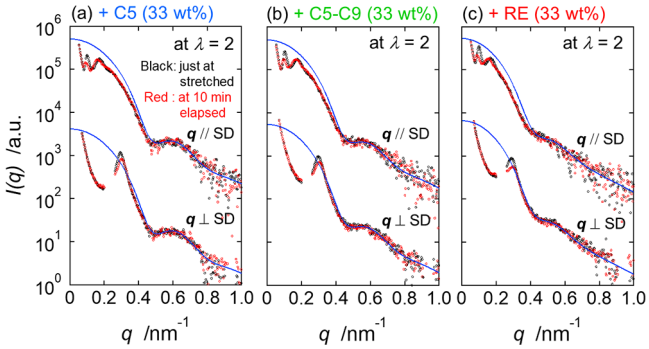

Figure 5. 1D-SAXS profiles for the SIS/SI-tackifier specimens (tackifier content: 33 wt %) stretched at $\lambda = 2$. The tackifiers are (a) C5 resin, (b) C5−C9 resin, and (c) RE resin. Those profiles were obtained from the through-view 2D-SAXS patterns (shown in Figure S4 in the Supporting Information) by conducting the sector average. Note that the sector average was conducted with the azimuthal angle range of $\mu = 90° \pm 1°$ and $\mu = 0° \pm 1°$ for the $\boldsymbol{q}$ direction parallel to SD ($\boldsymbol{q}$ // SD) and perpendicular to SD ($\boldsymbol{q} \perp$ SD), respectively. The definition of μ is given in Figure S3a1. Note here that the black symbols show the profiles obtained just after reaching the stretched state, while the red symbols show the one obtained at 10 min elapsed.

in $\boldsymbol{q}$ // SD shifted toward the lower q region, while in $\boldsymbol{q} \perp$ SD, the first-order peak shifted toward the higher q region. The results of the detailed analysis are summarized in Table S1 in the Supporting Information, including the results for the SIS/SI neat specimens. It is found that the d spacing in $\boldsymbol{q}$ // SD increased while the d spacing in $\boldsymbol{q} \perp$ SD decreased during 10 min from the onset of the stretched state at $\lambda = 2$. This means the proceeding of the bcc lattice deformation. Furthermore, the intensity of the first-order peak was found to decrease during 10 min from the onset of the stretched state at $\lambda = 2$. This clearly indicates the decrease of the number of the {110} planes of the bcc lattice during 10 min with almost no change in the number of the {211} planes. Note that, since there is no change in the particle scattering peak (the peak position and intensity), it can be assumed that the PS sphere is not deformed nor broken at lower stretching ($\lambda = 2$). To comprehensively explain these results, we examined the azimuthal angle dependence of the {110} reflection peak intensity in the following paragraph.

Figure 6b−d shows the azimuthal angle (μ) dependence of peak intensity of the {110} reflection (the first-order peak) for the SIS/SI-tackifier specimens (tackifier content: 33 wt %) stretched at $\lambda = 2$, obtained from the 2D-SAXS patterns shown in Figure S4 in the Supporting Information. The appearance of four maximum positions in panels (b−d) is typical of a stretched specimen bearing spherical microdomains arranged in the bcc lattice being oriented toward the SD with the <110> direction parallel to SD.[36] The fact that, at 10 min elapsed, the peak intensity of the {110} reflection decreased indicates that the number of {110} planes satisfying the reflection condition with $\boldsymbol{q}$ // SD decreased. This further implies the orientation of the {110} planes proceeding as a function of the idling time. As a matter of fact, the maximum positions of the black curves in Figure 6b−d shifted from $\mu = 35$ to 30° and from $\mu = 146$ to 151° (C5), from $\mu = 42$ to 37° and from $\mu = 141$ to 146° (C5−C9), and from $\mu = 45$ to 38° and from $\mu = 138$ to 143° (RE) during the 10 min idling time. This means that the grain is rotating to orient more the bcc lattice with the <111> direction parallel to SD. Figure 6h shows the μ dependence of

https://doi.org/10.1021/acsomega.1c01367
ACS Omega 2021, 6, 17299−17313

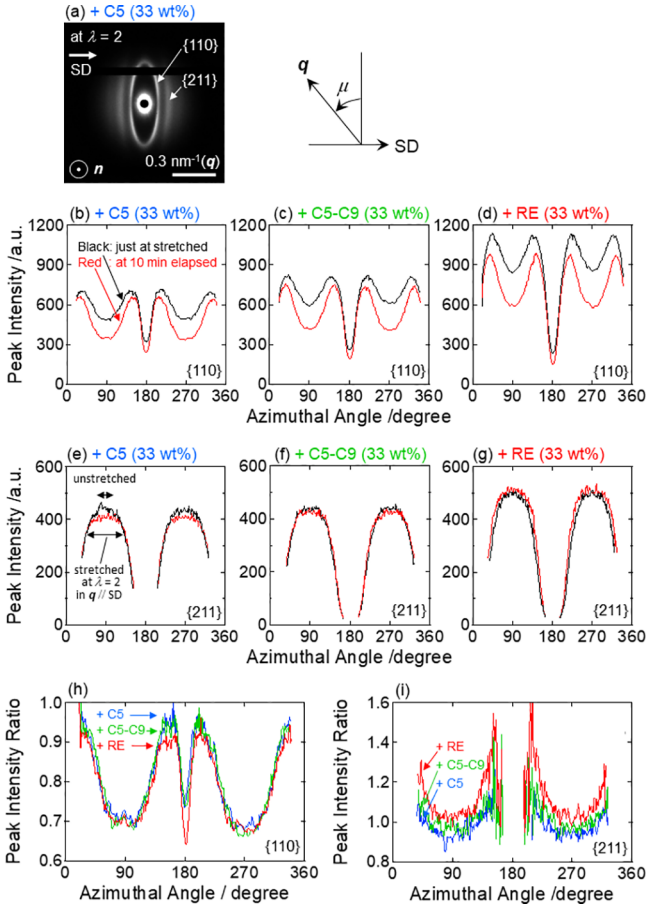

Figure 6. Panel (a) is an example of the 2D-SAXS pattern (for the SIS/SI-C5 resin specimen) to specify the reflection peaks due to {110} and {211} planes. The definition of azimuthal angle (μ) is shown together. Panels (b–d) and panels (e–g) show μ dependence of the peak intensity of the {110} and {211} reflection, respectively, for the SIS/SI-tackifier specimens (tackifier content: 33 wt %) stretched at λ = 2, obtained from the 2D-SAXS patterns shown in Figure S4 in the Supporting Information. The tackifiers are (b, e) C5 resin, (c, f) C5–C9 resin, and (d, g) RE resin. Panels (h) and (i) show μ dependence of the peak intensity ratio (I_{10min}/I_{0min}) for {110} and {211} reflections shown in panels (b–d) and (e–g), respectively. Here, I_{0min} and I_{10min} designate the peak intensity measured at just after reaching the stretched state (black curves in panels (b–g)) and 10 min elapsed (red curves in panels (b–g)), respectively.

the peak intensity ratio (I_{10min}/I_{0min}) estimated from the results of Figure 6b–d. Then, it was found that the peak intensity decreased by about 30% in all the specimens in $\boldsymbol{q}$ // SD (μ = 90 or 270°) and $\boldsymbol{q}$ ⊥ SD (μ = 0 or 180°) due to the progress of the orientation of the bcc lattice. The SIS/SI-RE resin specimen shows the lowest peak intensity ratio in the $\boldsymbol{q}$ direction perpendicular to SD ($\boldsymbol{q}$ ⊥ SD) (μ = 180°). This is probably because the RE resin is dissolved most in the PS spheres and plasticizes them so that PS chains can be easily pulled out from the PS spheres, which enables the rotation of grains, promoting more orientation of the bcc lattice.

Figure 6e–g shows the μ dependence of the peak intensity of the {211} reflection for the SIS/SI-tackifier specimen (tackifier content: 33 wt %) stretched at λ = 2. Similar to the case of the {110} reflection in Figure 6h, the change of its intensity during the 10 min idling time is examined in Figure 6i where the μ dependence of the peak intensity ratio (I_{10min}/I_{0min}) is plotted. Opposite to the case of the {110} reflection, it was clearly found that the intensity of the peak due to the {211} reflection planes was not decreased so much and even the intensity was increased in the case of the RE resin. We should consider the same scheme to understand the behavior of the change in the intensity of the {211} plane reflection. The following figure (Figure 7) considers the affine

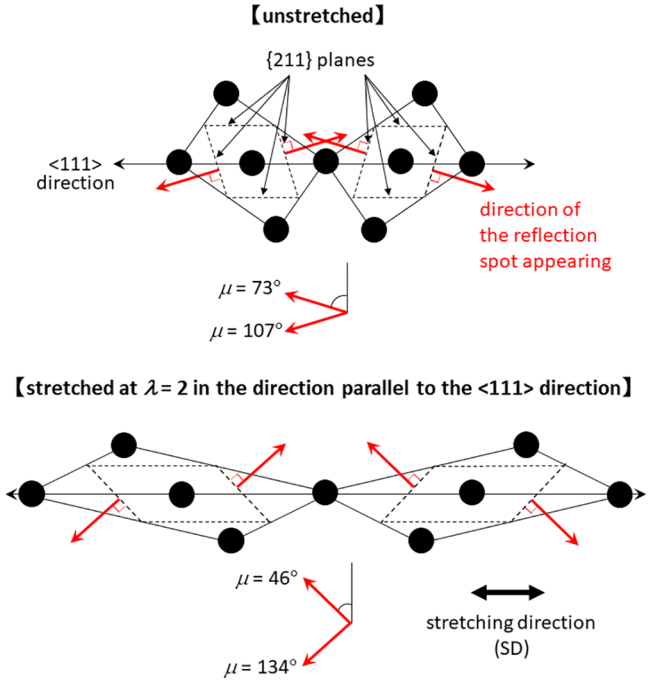

Figure 7. Schematic illustration of an affine deformation of a bcc lattice in which the <110> direction is parallel to SD before stretching and at the uniaxially stretched state with λ = 2.

deformation of the ordered spherical microdomains when the original bcc lattice is uniaxially stretched in the direction parallel to the <111> direction. Since the nearest-neighboring spheres are arranged on the <111> direction, this axis has a higher chance to be oriented parallel to SD. According to the schematic illustrations shown in Figure 7, the {211} reflection peaks should appear in the directions with μ = 73, 107, 253, and 287° when the bcc lattice is perfectly oriented with the <111> direction completely parallel to SD. Then, these reflection spots should move to the azimuthal angle μ = 46, 134, 226, and 314° upon the uniaxial stretching at λ = 2. The initial specimen showed the 2D-SAXS patterns with the isotropic peaks of the {110} and {211} reflections, which suggest the random orientation of the bcc lattice. Upon the uniaxial stretching of the specimen, the <111> direction of the bcc lattice can be considered to start orienting so that the black curves in Figure 6e–g showed the typical distribution of the peak intensity as a function of μ (two broad peaks at μ = 90 and 270°). Instead of showing individual peaks at μ = 73, 107, 253, and 287°, the black curves showed broad peaks in the μ ranges with 60° < μ < 120° and 240° < μ < 300°. This indicates that the bcc lattice orientation was not perfectly completed at the timing of just after reaching the stretched state. It is considered that the orientation will gradually proceed during the 10 min idling time. As a matter of fact, the red curve in Figure 6e showed the widening of the peaks with decreasing intensity around μ = 90 and 270°. It is also noteworthy that the widened peaks in the red curves are

https://doi.org/10.1021/acsomega.1c01367
ACS Omega 2021, 6, 17299–17313

located in the ranges of 46° < μ < 134° and 226° < μ < 314°, which are completely in good accord with the azimuthal angles at which spots of the {211} peaks should appear in the case of complete orientation of the bcc lattice with respect to <111> // SD with λ = 2. Nevertheless, the fact that the red curve still showed the broad peaks instead of four spots indicates that the orientation of the deformed bcc lattice was in progress. Similarly, the decreasing of the peak intensity around μ = 90 and 270° ensures the progress of the orientation of the deformed bcc lattice. Although this typical behavior was not clear in the case of the C5−C9 resin (Figure 6f) and in the case of the RE resin (Figure 6g), for which the intensity was even increased in the whole range of the azimuthal angle, the peak intensity ratio shown in Figure 6i clearly indicates a similar tendency for all the cases. This ensures the progress of the orientation of the deformed bcc lattice during the 10 min idling time for all the cases. Furthermore, the downward parabolic shape in the case of the RE resin was sharpest among the three cases. This may suggest that the superior progress of the deformed bcc orientation is ascribed to the plasticizing effect of the RE resin on the glassy PS spheres.

The {110} reflection peak (the first-order peak) at μ = 90 or 270° is closest to the center, which means that the specimen was stretched in that direction (see the μ dependence of the peak position of the {110} reflection in Figure S5 in the Supporting Information). The position of the first-order peak at μ = 90° ($\boldsymbol{q}$ // SD) and μ = 180° ($\boldsymbol{q}$ ⊥ SD) just after reaching the stretched state at λ = 2 were q = 0.098 nm (C5), 0.102 nm (C5−C9), and 0.099 nm (RE) and q = 0.290 nm (C5), 0.298 nm (C5−C9), and 0.285 nm (RE), respectively. Since these are almost half ($q_{//}/q_0$ = 1/2) and $\sqrt{2}$ times ($q_{\perp}/q_0 = \sqrt{2}$) of the unstretched q values [q_0 = 0.196 nm (C5), 0.203 nm (C5−C9), and 0.198 nm (RE)],[20] it was confirmed that the bcc lattice was deformed according completely to the affine deformation with keeping the volume of the specimen constant.[37,38] The further shift of the peak positions shown in Figure 5 and Table S1 in the Supporting Information during the 10 min idling time at λ = 2 clearly indicates the further progress in the microscopic stretching. The reduction of the peak intensity is in the order of C5 = C5−C9 < RE, and the PS spherical microdomain is plasticized in a similar order. This intriguing phenomenon suggests the pulling out of PS chains from PS spherical microdomains even at such a low stretching ratio as λ = 2. Due to the physical entanglement of mid-PI chains, some of the mid-PI chains are considered to suffer from a highly stretched state. When the cohesive force in the PS phase is weakened by the addition of the tackifier molecules, the PS chain connected to such a highly stretched mid-PI chain may be pulled out. It is also notable that the particle scattering peak is broader for the SIS/SI-tackifier specimens as compared to that of the SIS/SI neat specimen. This clearly indicates that the distribution of the sphere radius is wider for the SIS/SI-tackifier specimens, resulting from the inhomogeneous distribution of the tackifier molecules in the specimens. In this situation, there are appreciable amounts of small PS spheres in which the cohesive force of the PS chains is weak. Thus, the PS chains in such a small PS sphere may be easily pulled out even at a low stretched state. Once the chain pulling out occurs, the distance between the PS spheres connected by such a chain can be a bit increased. Thus, the microscopic stretching proceeds. Upon the event of the chain pulling out, the small PS sphere becomes smaller, which might be detected by SAXS. However, the particle scattering intensity is proportional to the square of the volume of the sphere. Therefore, the decrease in the scattering intensity due to the disappearance of the original small sphere is trivial, while the increase in the scattering intensity due to the appearance of the smaller sphere is more trivial. Thus, the particle scattering seems to be unchanged after 10 min elapsed, as shown in Figure 5 for all of the specimens. It is clear that the particle scattering peak is most ambiguous for the SIS/SI-RE resin specimen, suggesting the very wide distribution in the radius of the PS sphere. This means that the occurrence of the pulling out of the PS chains is most frequent. As a matter of fact, the extent of the progress in the microscopic stretching in this specimen (SIS/SI-RE resin) is the largest.

Subsequently, the changes in the nanostructures in the specimens with a higher tackifier content were investigated. Figure 8 shows the 1D-SAXS profiles for the SIS/SI-tackifier specimens (tackifier content: 50 wt %) stretched at λ = 2. Those profiles were obtained from the through-view 2D-SAXS patterns (shown in Figure S5 in the Supporting Information). The panels (a′−c′) show the expanded views to focus on the temporal change in the profile around the main peak (due to the {110} reflection). In the 1D-SAXS profile in the case of the lower stretching (λ = 2) as shown in Figure 8a−c, the first-order peak is very difficult to detect, but it exists at around q = 0.1 nm^{-1} (in the 1D-SAXS profiles for the SIS/SI-RE resin and SIS/SI-C5C9 resin specimens). On the contrary, it almost disappeared in the 1D-SAXS profile for the SIS/SI-C5 resin as shown in the expanded views in Figure 8a′−c′. This may be due to the high orientation of the deformed bcc lattice. At 10 min elapsed, the third-order peak ($\sqrt{6}$ peak) as a shoulder

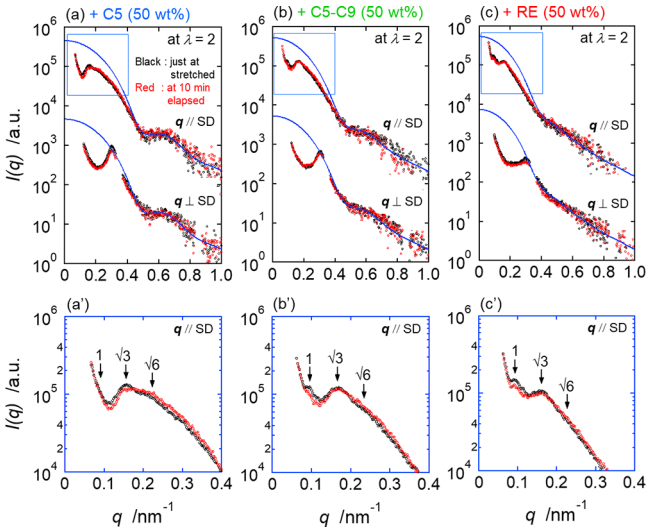

Figure 8. 1D-SAXS profiles for the SIS/SI-tackifier specimens (tackifier content: 50 wt %) stretched at λ = 2. The tackifiers are (a) C5 resin, (b) C5−C9 resin, and (c) RE resin. Those profiles were obtained from the through-view 2D-SAXS patterns (shown in Figure S5 in the Supporting Information) by conducting the sector average. Note that the sector average was conducted with the azimuthal angle range of μ = 90° ± 1° and μ = 0° ± 1° for the $\boldsymbol{q}$ direction parallel to SD ($\boldsymbol{q}$ // SD) and perpendicular to SD ($\boldsymbol{q}$ ⊥ SD), respectively. The definition of μ is given in Figure 6a. Note here that the black symbols show the profiles obtained just after reaching the stretched state, while the red symbols show the one obtained at 10 min elapsed. The panels (a′−c′) show the expanded views to focus on the temporal change in the profile around the main peak (due to the {110} reflection).

https://doi.org/10.1021/acsomega.1c01367
ACS Omega 2021, 6, 17299−17313

became discernible, suggesting that the orientation progressed. The shift of these peaks at 10 min elapsed was not so clear as that found in Figure 5, while the intensity of the first-order peak was decreased for both q directions of $\boldsymbol{q}$ // SD and $\boldsymbol{q} \perp$ SD. As compared to the specimens with 33 wt % addition of the tackifier (Figure 5), the pulling out of the PS chains should more frequently occur because of the more weakened cohesive force in the PS phase due to the higher tackifier content for the specimens with 50 wt % addition of the tackifier (Figure 8). Thus, the particle scattering peak should be changed during the 10 min idling time. However, the change in the particle scattering peaks shown in Figure 8 is not discernible due to the poor statistical accuracy. The fact that the shift of the first-order peak is trivial for the specimens with C5−C9 and RE resins should indicate no occurrence of the pulling out of the PS chains. However, it is not true as mentioned above. As a matter of fact, the decrease in the intensity of the first-order peak suggests the promotion of the orientation of the bcc lattice during the 10 min idling time, which in turn suggests the occurrence of the pulling out of the PS chains.

2.3. Stress-Relaxation Behavior. Figure 9a shows the stress-relaxation curves for the SIS/SI neat specimen stretched at λ = 2, 10, and 13. To check the relative relaxation behavior, Figure 9b shows the relaxation of the normalized stress (σ/σ_0), where σ_0 denotes the initial value of the stress at t = 0. Dolle et al. reported that the mobility of molecular chains decreases with stretching at λ < 2 for the ethylene propylene dienemonomer (EPDM) cross-linked rubber.[39] It is quite interesting to see the peculiar behavior of the relaxation with respect to λ. The relaxation was fastest at λ = 2, the next was at λ = 13, and then it was slowest at λ = 10, i.e., not in the increasing order of λ. To understand such peculiar behaviors of the stress relaxation, parameter fitting with exponential decay functions was examined. Consequently, it was found that triple exponential decay functions (eq 1) can work well Figure 9. Uozumi et al. utilized the double exponential decay function (fast relaxation and slow relaxation) to fit the experimental results.[38] Tada et al. fitted the experimental data by five-component exponential functions (although there were no detailed explanations of each term).[40] In our current study, we were able to explain the stress-relaxation behavior by fitting with the following three-component exponential functions.

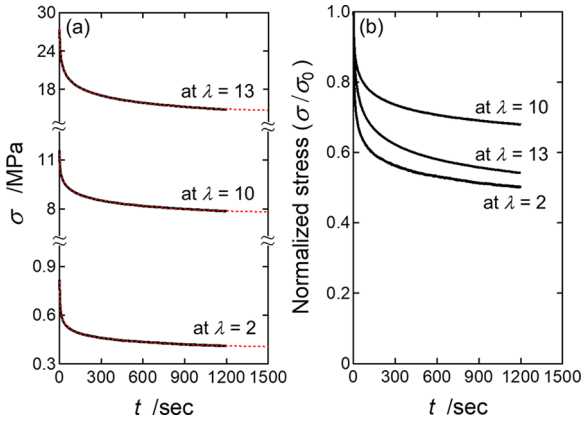

Figure 9. (a) Stress-relaxation curves for the SIS/SI neat specimen stretched at λ = 2, 10, and 13. Note that the red broken curves indicate the model fitting results using eq 2 refined from eq 1 in the main text. (b) Relaxation of the normalized stress (σ/σ_0), where σ_0 denotes the initial value of the stress at t = 0.

$$\sigma(t) = \sigma_a \cdot \exp(t/\tau_a) + \sigma_b \cdot \exp(t/\tau_b) + \sigma_c \cdot \exp(t/\tau_c) + \sigma_{const} \quad (1)$$

Here, σ_K and τ_K are the prefactor and relaxation time for K = a, b, or c ($\tau_a < \tau_b < \tau_c$). σ_{const} is the remaining stress.

Figure 10 shows the stress-relaxation curves for the SIS/SI-tackifier specimens with various tackifier contents, stretched at (a) λ = 2, (b) λ = 10, and (c) λ = 15. Likely for the SIS/SI neat specimen, eq 2 refined from eq 1 described below was utilized to express the stress-relaxation behaviors for the SIS/SI-tackifier specimens. The triple exponential decay functions indicate the hierarchy of the structures that are the origins of the "fast mode" relating to the local relaxation due to the rotation of the repeating unit of polymer chains; the "intermediate mode" of the disentanglement of the mid-PI chains; and the "slow mode" relating to, in this particular case, pulling out of the PS chains from the PS sphere. The relaxation times (τ_a, τ_b, and τ_c) were found to be approximately 1:10:100 (τ_a = around 5−10 s) (see Figure 11). The "intermediate mode" due to the disentanglement of the mid-PI chains may involve not only the mid-PI bridge chains but also the mid-PI loop chains of the triblock copolymer and PI corona chains of SI in the base polymer of the specimens used in the current study, in which the corona chains are relaxed faster. In fact,

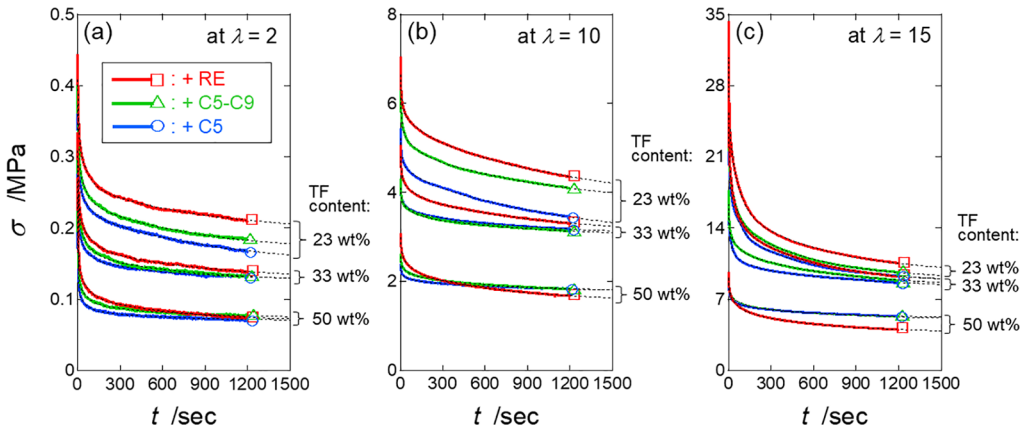

Figure 10. Stress-relaxation curves for the SIS/SI-tackifier specimens with various tackifier contents, stretched at (a) λ = 2, (b) λ = 10, and (c) λ = 15. Note that the black broken curves indicate the best-fit results using eq 2 in the main text.

https://doi.org/10.1021/acsomega.1c01367
ACS Omega 2021, 6, 17299−17313

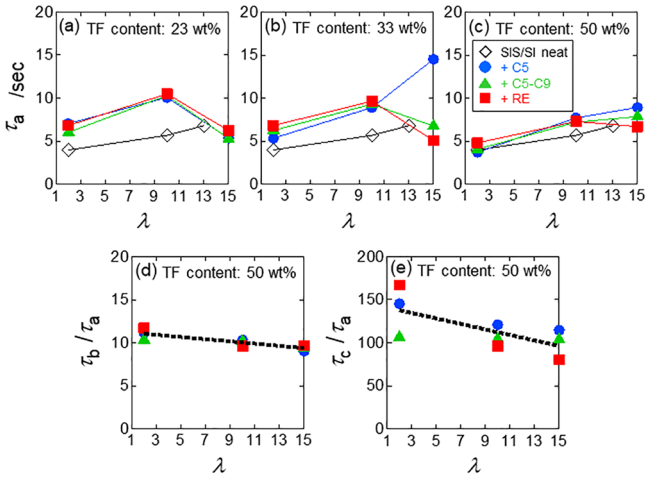

Figure 11. Plots of the fast-mode relaxation time τ_a as a function of λ for the SIS/SI-tackifier specimens, including the results for the SIS/SI neat specimen (a−c). Note that the τ_a was evaluated by fitting to the stress-relaxation curves using eq 1 in the main text. The tackifier contents are (a) 23, (b) 33, and (c) 50 wt %. Panels (d) and (e) show plots of the ratios of the relaxation times; (d) τ_b/τ_a and (e) τ_c/τ_a as a function of λ for the SIS/SI-tackifier specimens (tackifier content: 50 wt %). Here, τ_a, τ_b, and τ_c are the relaxation times ($\tau_a < \tau_b < \tau_c$) that were evaluated by fitting to the stress-relaxation curves using eq 1 in the main text. Refer to Figure S8 in the Supporting Information for the ratios (τ_b/τ_a and τ_c/τ_a) for the specimens with the tackifier contents of 23 and 33 wt %. Note that the thick broken lines indicate the approximate lines for all of the plots in each panel. Such approximated values of τ_b/τ_a and τ_c/τ_a obtained from these approximate lines were then substituted into eq 2 in the main text, and fitting to the stress-relaxation curves (as shown with broken curves in Figures 9 and 10) using eq 2 was performed again to refine the best fitted values of σ_a, σ_b, σ_c, and σ_{const}. Note here that upon fitting using eq 2, the value of τ_a was fixed at the best-fit one shown in panels (a−c).

Uozumi et al.[38] fitted the stress-relaxation behavior with two relaxation times and found that the longer relaxation time was about 50 s (the shorter relaxation time was about 5 s), which is consistent with the relaxation-time orders of τ_a and τ_b in the current study. Also, it has been reported that the molecular mechanism responsible for the relaxation process with several tens of seconds of relaxation time is the diffusion of dangling chain ends in the presence of entanglements in the case of the polymer network that is chemically cross-linked.[41−43] Such relaxation of the dangling chain corresponds to the relaxation of the loop chain of SIS (although no chain ends are relevant) and the corona chain of SI in the base polymer of the specimens used in the current study. Note here that there are two representatives of the entanglement of the mid-PI chains (irrespective of the loop or bridge conformation), which are easily unraveled or permanently locked. Although it is considered that the latter cannot be unraveled forever, the latter can be also unraveled when the PS-end chains, which are kinetically locked in the glassy PS spheres, are pulled out of the spheres. This event more frequently happens when the specimen is stretched to a higher extent because the mid-PI chains undergo high stretching and pulling out of the end-PS chains with higher force. Such pulling out of the end-PS chains relaxes the stress and contributes as the "slow relaxation mode" to the stress-relaxation behavior of the physically cross-linked polymer network.

$$\sigma(t) = \sigma_a \cdot \exp(t/\tau_a) + \sigma_b \cdot \exp[t/\{(\tau_b/\tau_a)\tau_a\}] + \sigma_c \cdot \exp[t/\{(\tau_b/\tau_a)\tau_a\}] + \sigma_{const} \quad (2)$$

The corresponding plots of the relaxation of the normalized stress (σ/σ_0) were shown in Figure S7 in the Supporting Information. Roughly speaking, the remaining stress was in the order of RE < C5−C9 < C5 in the reverse order of the relaxation of the true stress in Figure 10. Such tendency correlates with the cohesive force in the PS phase. For instance, the high amount of the RE resin was solubilized in the PS phase so that easiness of the pulling out of the PS chains and in turn the easiness of the stress relaxation resulted for the SIS/SI-RE resin specimens.

Figure 11a−c shows the plots of the fast-mode relaxation time τ_a as a function of λ for the SIS/SI-tackifier specimens, including the results for the SIS/SI neat specimen. The relaxation time of the local motion of the PI repeating unit ranges from 5 to 10 s. The SIS/SI neat specimen without the tackifier has the shortest relaxation time because of no friction of the polymer segment with the tackifier molecules. However, the viscosity of the PI matrix may also affect τ_a, which is decreased with an increase in the tackifier content (Figure 11a−c). It is noteworthy that τ_a increases with λ for the SIS/SI neat specimen. This may be ascribed to the slight increase in the friction between segments of the oriented polymer chains at higher λ (or a confinement effect upon the decrease in the lateral size of the test piece, i.e., in both width and thickness). As for the SIS/SI-tackifier specimens, overall, there is no appreciable difference in τ_a behaviors independent of the types of the tackifier because of no chemical aspect affecting the τ_a behaviors. At the highly stretched state at $\lambda = 15$, there would be a tendency that τ_a decreases. Since the loop mid-PI chains can be oriented due to the physical entanglement of the loop chains (never disentangled feature), the loop chain can contribute to the tensile stress. Slippage of the entanglement point may shorten τ_a.

Since it is expected that there would be a strong correlation among τ_a, τ_b, and τ_c, the ratios of τ_b/τ_a and τ_c/τ_a are examined in Figure 11d,e where (d) τ_b/τ_a and (e) τ_c/τ_a are plotted as a function of λ for the SIS/SI-tackifier specimens (tackifier content: 50 wt %). The thick broken lines indicate the approximate lines for all of the plots in each panel. Refer to Figure S8 in the Supporting Information for the ratios (τ_b/τ_a and τ_c/τ_a) for the specimens with the tackifier contents of 23 and 33 wt %. Thus, the τ_b and τ_c were found to be about 10 times (around 50−100 s) and 120 times (around 600−1200 s) of τ_a, respectively. To refine the behaviors of the prefactors σ_a, σ_b, and σ_c, the parameter fitting utilizing eq 1 was now re-examined by utilizing eq 2 using the approximated values of τ_b/τ_a and τ_c/τ_a as shown in Figure 11d,e with the thick broken lines. Note here that upon the fitting using eq 2, the value of τ_a was fixed at the one shown in Figure 11a−c.

Based on thus-evaluated values for σ_a, σ_b, σ_c, and σ_{const} from the parameter fitting, the fractions of σ_a, σ_b, σ_c, and σ_{const} (%) were plotted in Figure 12 as a function of λ for the SIS/SI-tackifier specimens, including the results for the SIS/SI neat specimen. The tackifier contents are 23 wt % for panels (a-1) to (d-1), 33 wt % for panels (a-2) to (d-2), and 50 wt % for panels (a-3) to (d-3). Here, the respective fractions (%) are calculated by $\sigma_x/(\sigma_a + \sigma_b + \sigma_c + \sigma_{const}) \times 100$ with σ_x (x = a, b, c, const). First of all, we will discuss the fraction of the remaining stress, σ_{const} (Figure 12d1−d3). The fraction of σ_{const}

https://doi.org/10.1021/acsomega.1c01367
ACS Omega 2021, 6, 17299−17313

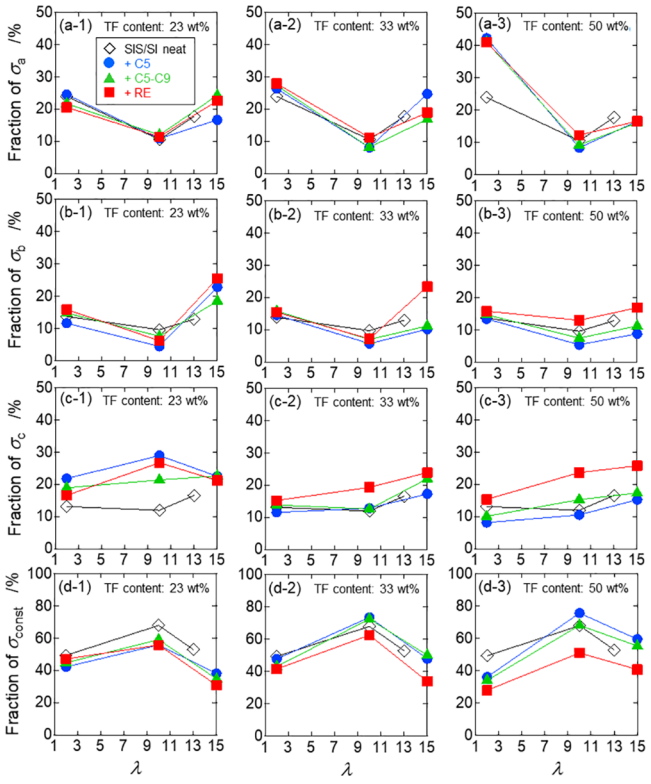

Figure 12. Plots of fractions of σ_a, σ_b, σ_c, and σ_{const} (%) (which were refined by the fitting using eq 2 in the main text) as a function of λ for the SIS/SI-tackifier specimens, including the results for the SIS/SI neat specimen. The tackifier contents are 23 wt % for panels (a-1) to (d-1), 33 wt % for panels (a-2) to (d-2), and 50 wt % for panels (a-3) to (d-3).

exhibited a parabolic shape with the highest value at $\lambda = 10$ irrespective of the type of the tackifier and its concentration. As an overall tendency, it can be recognized that the fraction of σ_{const} increased with the increase of λ. But at $\lambda = 15$, due to the contribution of the entangled loop chains of the mid-PI, the stress can be more relaxed. The fact that the case of the RE shows the lowest σ_{const} is ascribed to the easy chain pulling out. As for the fraction of σ_a, it shows the minimum at $\lambda = 10$. This means that the fast mode of the stress relaxation due to the local motion of the repeating unit of polymer chains is not the main contribution at $\lambda = 10$, which may be ascribed to the above-mentioned confinement effect. The fraction of σ_b has a similar tendency. Since the σ_b fraction is ascribed to the stress relaxation by the chain disentanglement, this contribution can be increased at $\lambda = 15$ because of the easy disentanglement due to the higher stress. The fraction of σ_c exhibited a tendency to increase monotonically with λ. Since this stress relaxation is ascribed to the chain pulling out from the PS sphere, the higher occurrence of this phenomenon at $\lambda = 15$ is reasonable. Furthermore, this contribution for the SIS/SI-RE resin is the highest. This is also reasonable because of its weakest cohesive force in the PS phase. There is one exception of the behavior at $\lambda = 15$ for the tackifier content of 23 wt % (C5 and RE cases), showing lower values of σ_c as compared to those at $\lambda = 10$. This is due to the countereffect of the increase in the σ_b fraction. For these particular cases, the higher stress acting on the mid-PI chains with loop conformation mainly induces the disentanglement so that the larger fraction of σ_b resulted. Then, the fraction of σ_c was relatively decreased, which may be a plausible explanation of the exceptional behaviors in Figure 12c-1 in the case of C5 and RE resins.

2.4. Relaxation Spectrum Evaluated by Linear Viscoelastic Measurements. Although we can fit the relaxation process of the tensile stress with the three-component exponential function, this treatment is just phenomenological. To appropriately understand the wide distribution of the relaxation times of specimens, it is highly recommended to conduct an evaluation of the relaxation spectrum based on the linear viscoelastic measurements of the storage shear modulus (G') as a function of the dynamic frequency (ω) with the dynamic strain amplitude of 0.001. Figure 13 shows the resulting master curves of $G'(\omega)$ for the

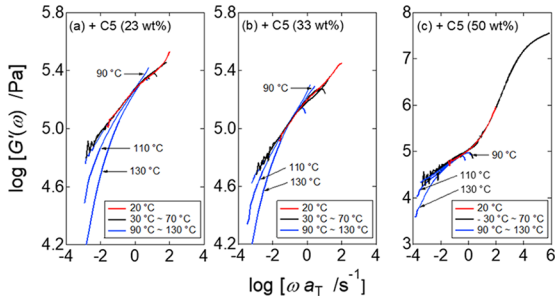

Figure 13. Master curves of $G'(\omega)$ for the specimens with C5 resin having (a) 23 wt %, (b) 33 wt %, and (c) 50 wt % contents.

three representative specimens with the C5 resin. Note that the raw data (Figure S9 in the Supporting Information) were horizontally shifted in a double logarithmic plot of G' and ω to obtain a good overlap to the data obtained at 20 °C. The reason to choose 20 °C as the reference temperature is because this temperature is closest to the temperature (23 °C) of the measurements of the tensile stress relaxation. For the specimens with 23 and 33 wt % tackifier contents, the master curves can be obtained by using the data measured in the range of 20−70 °C. As shown in Figure 13a,b, the data measured at 90 °C exhibited branching in the higher-frequency region, although a good overlap was obtained in the lower-frequency region. As for the data measured at 110 and 130 °C, they clearly exhibited downward deviations from their master curves, implying macroscopic flow of these specimens, which further implies the rubbery behavior of PS spheres at those temperatures because the measuring temperatures were higher than $T_{g,PS}$. Thus, the data in the range of 90−130 °C were excluded for the master curve estimation. As for the specimen with 50 wt % tackifier content, it was found that the data obtained in the cooler temperature range (−30 and −10 °C) can be used. However, the Arrhenius plots shown in Figure 14 exhibited a completely different behavior from that in the temperature range of 20−70 °C where almost identical slopes were obtained for all of the specimens. Note that the slope correlates with the activation energy of the relaxation and that it is higher in the cooler temperature range than in the temperature range of 20−70 °C. Thus, we decided to use the master curves obtained using data in this temperature range for the further evaluation of the relaxation spectra.

Figure S10 in the Supporting Information shows the smoothing of the master curves by using polynomial-function fitting (up to the term of $(\log[a_T\omega])^9$) to obtain the smoothed results of the relaxation spectra ($H(\tau)$), as shown in Figure 15, which were evaluated according to the following equation:[44]

https://doi.org/10.1021/acsomega.1c01367
ACS Omega 2021, 6, 17299−17313

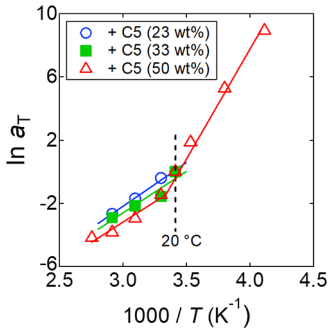

Figure 14. Arrhenius plots of the shift factor a_T for the specimens with C5 resin having 23−50 wt % contents.

$$H(\tau) = G'(\omega)/d \ln \omega|_{\tau=1/\omega} \quad (3)$$

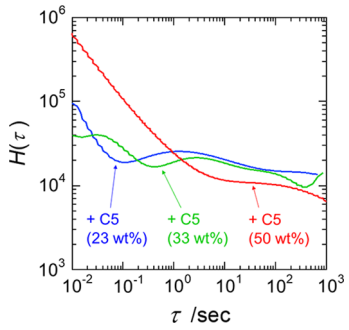

Figure 15. Relaxation spectra ($H(\tau)$) for the specimens with C5 resin having 23−50 wt % contents.

For the specimen with 23 wt % tackifier content, it was found that two peaks appeared at τ = 1.5 and 335 s. Additionally, it would be suggested that a hidden peak exists at around 10 s. These three relaxation times were found to closely correspond to three representative relaxation times found in the tensile stress relaxation measurements by taking into account the very contrasting difference in the strain (amplitude) between two kinds of measurements (0.001 and 1−14). The broad peak at τ = 1.5 s can be considered as stress relaxation due to the quick motion of the segments of the mid-PI chains. Nevertheless, the continuous spectrum around τ = 1−10 s reminds the stress relaxation of the deformed uncrosslinked polymer network.[45] Namely, the deformed mid-PI chains (with both the bridge and loop conformations) can be considered to relax. Some mid-PI chains, which roughly entangle, would be responsible for this relaxation. On the contrary, the long relaxation time reflects the relaxation of the deformed hard PS spheres because there is no peak in such a long-relaxation time zone in the case of a simple uncrosslinked polymer.[45] Furthermore, it is noteworthy that the relaxation spectrum for the specimen with 23 wt % tackifier content does not exhibit a decreasing tendency in the longer-relaxation time zone. This clearly indicates that the specimen does not flow macroscopically, further implying that there may be a rare occurrence of the pulling out of the PS block chains from its spherical microdomains.

Since three peaks were found for the specimen with 33 wt % tackifier content at τ = 3.3, 100, and 900 s and a peak appeared at τ = 0.04 s, similar arguments for the specimen with 23 wt % tackifier content are applicable also to the specimen with 33 wt % tackifier content. On the contrary, the relaxation spectrum for the specimen with 50 wt % content exhibits very contrasting behavior, as it is similar to that for a simple uncrosslinked polymer. Actually, the relaxation spectrum exhibits a decreasing tendency in the longer-relaxation time zone, indicating the macroscopic flow of this specimen because of plasticization of the PS phase with the C5 resin in this specimen (although C5 is selective to PI, C5 molecules are considered to be solubilized in PS in some extent), as well as the resultant easy occurrence of pulling out of the PS block chains from the PS spherical microdomains. Thus, the onset time of this decreasing behavior at around 300 s can be considered as the longest relaxation time, which indicates the relaxation due to the disentanglement of the mid-PI chains triggered by the pulling out of the PS block chains. This relaxation time (τ = 300 s) corresponds to the longest relaxation time in the tensile stress relaxation behavior. Although the relaxation spectrum looks similar to that for entangled simple polymers, the slope of the power-law behavior of the relaxation spectrum in the lower-relaxation time zone for this specimen with 50 wt % tackifier content is −0.75, which is steeper than that in the case of the concentrated polymer solution (the slope is −0.5[46]). Additionally, the crossover relaxation time where the power-law behavior changes into the plateau behavior should be around the relaxation time of 1 s in the case of the entangled simple polymers, while the relaxation spectrum for this specimen indicates the crossover to be around 10 s. These facts may suggest that there is a hidden continuous relaxation spectrum in the relaxation time zone of 1−10 s. Such a hidden relaxation spectrum hopefully explains the fast and intermediate relaxation times of the tensile stress relaxation for the specimen with 50 wt % tackifier content.

3. CONCLUSIONS

We revealed the relationship between the mechanical properties and the structure of block copolymers mixed with tackifiers (C5, C5−C9, and RE resin) whose relative solubility to the respective components of styrenic block copolymers differs. For this purpose, the stress−strain and stress-relaxation measurement at various stretching ratios were performed. To clarify the correlation between the changes in the nanostructure and mechanical properties, we conducted an analysis of structural changes upon uniaxial stretching by 2D-SAXS measurements. As for stress−strain behavior, the Young's modulus and overall stress decreased in the order of C5 > C5−C9 > RE due to the decrease in PI-bridge chains (in the order of the content of tackifier in the PI matrix phase). We were able to explain the stress-relaxation behavior by fitting with the three-component exponent functions. The triple exponential decay functions indicate the hierarchy of the structures that are the origins of the "fast mode" relating to the local relaxation due to the rotation of the repeating unit of polymer chains; the "intermediate mode" of the disentanglement of the mid-PI chains; and the "slow mode" relating to, in this particular case, pulling out of the PS chains from the PS sphere. The largest amount of the RE resin was solubilized in the PS phase so that it can be considered that pulling out of the PS chains took place easily; as a result, the contribution of the slow-mode relaxation component increased. These tensile stress relaxation behaviors with three representative relaxation times were substantially confirmed with the relaxation spectra evaluated based on the linear viscoelastic measurements of $G'(\omega)$ in the temperature range of 20−70 °C for the specimens with the C5

https://doi.org/10.1021/acsomega.1c01367
ACS Omega 2021, 6, 17299−17313

resin with 23 and 33 wt % contents or in the temperature range of −30 to 70 °C for the specimens with the C5 resin with 50 wt % content.

4. EXPERIMENTAL SECTION

4.1. Materials and Methods. The materials used in this study are the block copolymers and tackifiers, which are the same materials used in our previous study (shown in Table 1).[20] The molecular characteristics of block copolymers and tackifiers are listed in Table 1. As the base polymer, a blend of the SIS triblock copolymer and SI diblock copolymer (SIS/SI) ("QUINTAC 3433N", Zeon Corp., Tokyo, Japan) was used. The three types of tackifiers were aliphatic resin (denoted as C5 and synthesized from monomers with five carbon atoms) ("QUINTON R100", Zeon Corp., Tokyo, Japan), the C5−C9 resin in which C5 and aromatic resin (denoted as C9 and synthesized from hydrocarbons containing mainly nine carbon atoms) are covalently bonded ("QUINTON DX390N", Zeon Corp., Tokyo, Japan), and rosin ester (RE) resin ("SUPER-ESTER A100", Arakawa Chemical Industries, Ltd., Osaka, Japan). The three types of tackifiers were added to the SIS/SI (SIS/SI-tackifier specimens), and the tackifier contents were 23, 33, and 50 wt % on the total solid (the ratios of the SIS/SI and the tackifier are 100/30, 100/50, and 100/100 by weight, respectively).

The preparation method for the coated layer specimens is the same as that used in our previous study[47] by solution coating with a final thickness of 50 μm after completely drying. The toluene solution of the SIS/SI-tackifier specimens was prepared at a solid concentration of 30 wt %. Then, the solution was coated on the substrate using an applicator that can adjust the gap and homogenize its thickness. Finally, the solution layer was dried at 80 °C for 3 min in the oven with hot-air blow to evaporate the toluene. As a substrate, a silicon-coated polyethylene terephthalate film (Si-PET film, "PUREX", Toyobo Film Solutions Ltd., Tokyo Japan; 38 μm thick) was used. The as-coated layers were stacked to obtain thicker specimens suitable for stress−strain and stress-relaxation measurements with keeping the preparation conditions whose effects are still remaining in the test specimens. The final thickness of the stacked specimens was adjusted to 1 mm (for the detailed procedure of how to stack the as-coated layers, refer to our previous paper[47]). Note that the specimens were prepared just prior to stress−strain and stress-relaxation measurements. Also, for the 2D-SAXS measurements, the specimens subjected to the measurements were prepared and stored in a freezer (−20 °C) for a few days prior to the 2D-SAXS measurements that were conducted at room temperature at the SAXS beamline of KEK-PF (Photon Factory in High Energy Accelerator Research Organization, Tsukuba, Japan).

4.2. Stress−Strain Measurements. The S−S curves were measured using the tensile testing machine "RTG-1210" (A&D Co., Ltd., Tokyo, Japan). The stacked specimens (1 mm thick) were cut into rectangles 5 mm wide and 40 mm long. The tensile test was conducted at room temperature with an initial cross-head distance of 20 mm and a tensile rate of 300 mm/min in accordance with JIS Z 0237 (Japanese Industrial Standards). Note here that the result for each specimen is the average of the results of five successful measurements (by excluding the results of those measurements in which the test piece was broken down at the positions of the gripping jaws). The representative S−S curve was selected from the five successful curves to display the averaged S−S behavior among the five successful ones. Note that the S−S curve in this study represents the true stress curve, which was converted from the nominal stress curve by conducting corrections for the decrease in the cross-sectional area of the specimen as a function of strain. To calculate the true value of the λ, the displacement of the distance of two neighboring dots that are marked on the surface of the stacked specimens in advance was tracked by video recording. The initial interval between the two neighboring dots was set at 5.0 mm. As for the conversion from the nominal stress (σ_n) to the true value (σ), we assume that $\sigma = \sigma_n \times \lambda$. It is simply because $\sigma_n = F/A_0$ and $\sigma = F/A$, where F is the load and A_0 and A denote the cross-sectional area of the specimens before stretching and at the stretched state, respectively. Then, $\sigma = \sigma_n \times A_0/A = \sigma_n \times (V_0/l_0)/(V/l) = \sigma_n \times (l/l_0) = \sigma_n \times \lambda$ is derived by assuming that the specimen volume can be kept constant upon stretching ($V_0 = V$), where V_0 and V denote the volume of the specimen before stretching and at the stretched state, respectively, and l_0 and l denote the distance between two neighboring dots marked on the specimen before stretching and at the stretched state, respectively (see our previous paper[48]).

4.3. 2D-SAXS Measurements. 2D-SAXS measurements were conducted at the BL-15A2 beamline of KEK-PF. The specimens were cut into a rectangle (5 mm wide and 40 mm long). The specimens were stretched at a tensile rate of 1000 mm/min up to a given true-stretching ratio by using the compact tensile testing machine (ISUT-2207; IS Giken Co., Ltd., Kyoto, Japan) at room temperature with an initial cross-head distance of 20 mm. The through-view SAXS measurements for the central part of the stretched specimens were conducted with 2 s of X-ray exposure time in the case just at stretched or 20 s of X-ray exposure time in the case at 10 min elapsed from the onset of the stretched state at a given λ. PILATUS3 2 M-PF (Dectris Ltd., Baden, Swizerland) was used as a two-dimensional detector. The wavelength ($\lambda_{X\text{-ray}}$) of the X-ray was set at 0.1213 nm (10.222 keV), and the sample-to-detector distance was 3.5 m. q denotes the magnitude of the scattering vector [$q = (4\pi/\lambda_{X\text{-ray}}) \sin(\theta/2)$] with θ being the scattering angle, was calibrated using a chicken-tendon collagen with a d spacing of 65.3 nm.[49] As a background, the scattering from the empty specimen holder was measured and subtracted from the specimen scattering by taking into account the transmission of the specimen.

4.4. Stress-Relaxation Measurements. The stress-relaxation curves were measured using the same tensile tester used for the S−S measurements at 23 °C. The stacked specimens (thickness, 1 mm) were cut into a rectangle (5 mm wide and 40 mm long). The specimens were stretched at a tensile rate of 1000 mm/min up to a given true-stretching ratio (λ), and then the stress decay behaviors were measured for 20 min. Note that the specimen should be stretched as fast as possible; otherwise, relaxation begins during stretching. Therefore, the specimens were stretched at the maximum speed of the device capacity that was 1000 m/min. The SIS/SI-tackifier specimens were stretched up to λ = 2, 10, and 15, while the SIS/SI neat specimen was stretched up to λ = 2, 10, and 13 (instead of λ = 15 because the stretched specimen was broken during the stretching up to λ = 15).

4.5. Linear Viscoelastic Measurements. The shear viscoelastic behaviors of the SIS/SI-tackifier blend specimens were measured using "Physica MCR301" (Anton Paar Japan K.K., Tokyo, Japan) using a parallel-plate fixture. The stacked

https://doi.org/10.1021/acsomega.1c01367
ACS Omega 2021, 6, 17299−17313

specimens (thickness, 1 mm) were punched into a disk shape with a diameter of 20 mm. The frequency sweep (0.1−628 rad/s) of the viscoelasticity measurement was conducted with a strain amplitude of 0.001 in the temperature range of −30 to 130 °C (−30, −10, 10, 20, 30, 50, 70, 90, 110, and 130 °C).

■ ASSOCIATED CONTENT

Supporting Information

The Supporting Information is available free of charge at https://pubs.acs.org/doi/10.1021/acsomega.1c01367.

(1) Reduction of stress in the stress−strain behavior for the specimen of the SIS/SI with the tackifier; (2) structural changes upon uniaxial stretching of the SIS/SI neat specimen; (3) calculation of the model particle scattering profile by assuming Gaussian distribution for the sphere radius R; (4) structural changes upon uniaxial stretching of the SIS/SI-tackifier specimens (tackifier content: 33 wt %); (5) structural changes upon uniaxial stretching of the SIS/SI-tackifier specimens (tackifier content: 50 wt %); (6) stress relaxation curves of normalized stress (σ/σ_0) for the SIS/SI-tackifier specimens; (7) relationship of relaxation times (τ_b/τ_a and τ_c/τ_a) for the stress relaxation; and (8) results of the linear viscoelastic measurements for the SIS/SI-C5 resin specimens (PDF)

■ AUTHOR INFORMATION

Corresponding Author

Shinichi Sakurai − *Department of Biobased Materials Science, Kyoto Institute of Technology, Kyoto 606-8585, Japan; Department of Chemical Engineering, Indian Institute of Technology Guwahati, Guwahati, Assam 781-039, India;* orcid.org/0000-0002-5756-1066; Email: shin@kit.ac.jp

Authors

Takahiro Doi − *Advanced and Applied Research Institute, Nichiban Co., Ltd., Anjo, Aichi 446-8531, Japan;* orcid.org/0000-0003-1667-1186

Hideaki Takagi − *Photon Factory, High Energy Accelerator Research Organization, Tsukuba, Ibaraki 305-0801, Japan;* orcid.org/0000-0003-3389-7945

Nobutaka Shimizu − *Photon Factory, High Energy Accelerator Research Organization, Tsukuba, Ibaraki 305-0801, Japan;* orcid.org/0000-0002-3636-1663

Noriyuki Igarashi − *Photon Factory, High Energy Accelerator Research Organization, Tsukuba, Ibaraki 305-0801, Japan*

Complete contact information is available at: https://pubs.acs.org/10.1021/acsomega.1c01367

Notes

The authors declare no competing financial interest.

■ ACKNOWLEDGMENTS

This study was partially supported by Grant-in-Aid for Challenging Exploratory Research "Materials science on mille-feuille structure (MFS)—Development of next generation structural materials guided by a new strengthen principle" with Grant 18K19115 from the Ministry of Education, Culture, Sports, Science, and Technology of Japan. The SAXS experiments were performed at BL-15A2 in the Photon Factory, KEK, Japan (Approval 2017G672).

■ REFERENCES

(1) Quan, X.; Gancarz, I.; Koberstein, J. T.; Wignall, G. D. Effect of homopolymer molecular weight on the morphology of block copolymer/homopolymer blends. *Macromolecules* **1987**, *20*, 1431−1434.

(2) Hashimoto, T.; Tanaka, H.; Hasegawa, H. Ordered Structure in Mixtures of a Block Copolymer and Homopolymers. 2. Effects of Molecular Weights of Homopolymers. *Macromolecules* **1990**, *23*, 4378−4386.

(3) Likhtman, A. E.; Semenov, A. N. Theory of Microphase Separation in Block Copolymer/Homopolymer Mixtures. *Macromolecules* **1997**, *30*, 7273−7278.

(4) Prahsarn, C.; Jamieson, A. M. Morphological studies of binary homopolymer/block copolymer blends: effect of molecular weight. *Polymer* **1997**, *38*, 1273−1283.

(5) Listak, J.; Jia, X.; Plichta, A.; Zhong, M.; Matyjaszewski, K.; Bockstaller, M. R. Effect of block molecular weight distribution on the structure formation in block copolymer/homopolymer blends. *J. Polym. Sci., Part B: Polym. Phys.* **2012**, *50*, 106−116.

(6) Sakurai, S.; Irie, H.; Umeda, H.; Nomura, S.; Lee, H. H.; Kim, J. K. Gyroid Structures and Morphological Control in Binary Blends of Polystyrene-block-polyisoprene Diblock Copolymers. *Macromolecules* **1998**, *31*, 336−343.

(7) Lipic, P. M.; Bates, F. S.; Hillmyer, M. A. Nanostructured Thermosets from Self-Assembled Amphiphilic Block Copolymer/Epoxy Resin Mixtures. *J. Am. Chem. Soc.* **1998**, *120*, 8963−8970.

(8) Yamanaka, R.; Shimizu, N.; Igarashi, N.; Takagi, H.; Sakurai, S. Orienting cylindrical Microdomains in Polystyrene-*b*-Poly(Ethylene-*co*-Butylene)-*b*-Polystyrene Triblock Copolymer/Diluent Sheet by Application of Temperature Gradient. *Polimery* **2017**, *62*, 812−820.

(9) Tanaka, H.; Hasegawa, H.; Hashimoto, T. Ordered Structure in Mixtures of a Block Copolymer and Homopolymers. 1. Solubilizattion of Low Molecular Weight Homopolymers. *Macromolecules* **1991**, *24*, 240−251.

(10) Tanaka, H.; Hashimoto, T. Ordered Structures of Block Polymer/Homopolymer Mixtures. 3. Temperature Dependence. *Macromolecules* **1991**, *24*, 5713−5720.

(11) Koizumi, S.; Hasegawa, H.; Hashimoto, T. Ordered Structures of Block Copolymer/Homopolymer Mixtures. 5. Interplay of Macro- and Microphase Transitions. *Macromolecules* **1994**, *27*, 6532−6540.

(12) Bodycomb, J.; Yamaguchi, D.; Hashimoto, T. A Small-Angle X-Ray Scattering Study of the Phase Behavior of Diblock Copolymer/Homopolymer Blends. *Macromolecules* **2000**, *33*, 5187−5197.

(13) Harton, S. E.; Kumar, S. K. Mean-Field Theoretical Analysis of Brush-Coated Nanoparticle Dispersion in Polymer Materices. *J. Polym. Sci., Part B: Polym. Phys.* **2008**, *46*, 351−358.

(14) Meng, D.; Kumar, S. K.; Lane, J. M. D.; Grest, G. S. Effective Interactions between Grafted Nanoparticles in a Polymer Matrix. *Soft Matter* **2012**, *8*, 5002−5010.

(15) Wang, Y. C.; Kim, M. I.; Akasaka, S.; Saijo, K.; Hasegawa, H.; Hikima, T.; Takenaka, M. Fddd Structure in Polystyrene-*block*-polyisoprene Diblock Copolymer/Polystyrene Homopolymer Blends. *Macromolecules* **2016**, *49*, 2257−2261.

(16) Schmitt, M.; Hui, C. M.; Urbach, Z.; Yan, J.; Matyjaszewski, K.; Bockstaller, M. R. Tailoring Structure Formation and Mechanical Properties of Particle Brush Solid *via* Homopolymer Addition. *Faraday Discuss.* **2016**, *186*, 17−30.

(17) Doerk, G. S.; Yager, K. G. Rapid Ordering in "Wet Brush" Block Copolymer/Homopolymer Ternary Blends. *ACS Nano* **2017**, *11*, 12326−12336.

(18) Doerk, G. S.; Li, R.; Fukuto, M.; Yager, K. G. Wet Brush Homopolymers as "Smart Solvents" for Rapid, Large Period Block Copolymer Thin Film Self-Assembly. *Macromolecules* **2020**, *53*, 1098−1113.

(19) Chen, H. L.; Lin, S. Y.; Huang, Y. Y.; Chiu, F. C.; Liou, W.; Lin, J. S. Crystallization in the Vesicle Walls Templated by Dry-Brush Block Copolymer/Homopolymer Blend. *Macromolecules* **2002**, *35*, 9434−9440.

(20) Doi, T.; Takagi, H.; Shimizu, N.; Igarashi, N.; Sakurai, S. Effects of Solubility Difference of Tackifier to Respective Components of Block Copolymers on Microphase-Separated Structures in Coated Layers of Pressure-Sensitive Adhesive Prepared by Solution Coating Process. *ACS Appl. Polym. Mater.* **2020**, *2*, 4973−4984.
(21) Tomita, S.; Lei, L.; Urushihara, Y.; Kuwamoto, S.; Matsushita, T.; Sakamoto, N.; Sasaki, S.; Sakurai, S. Strain-Induced Deformation of Glassy Spherical Microdomains in Elastomeric Triblock Copolymer Films: Simultaneous Measurements of a Stress-Strain Curve with 2d-SAXS Patterns. *Macromolecules* **2017**, *50*, 677−686.
(22) Tomita, S.; Wataoka, I.; Igarashi, N.; Shimizu, N.; Takagi, H.; Sasaki, S.; Sakurai, S. Strain-Induced Deformation of Glassy Spherical Microdomains in Elastomeric Triblock Copolymer Films: Time-Resolved 2d-SAXS Measurements under Stretched State. *Macromolecules* **2017**, *50*, 3404−3410.
(23) Helfand, E.; Wasserman, Z. R. In: *Developments in Block Copolymers*; Goodman, I. Ed. Applied Science: New York, 1982, Chapter 4.
(24) Satas, D. *Handbook of Pressure-Sensitive Adhesive Technology*. Van Nostrand Reinhold Company Inc. 1982, Chapter 11.
(25) Sasaki, M.; Adachi, M.; Kato, Y.; Fujii, S.; Nakamura, Y.; Urahama, Y.; Sakurai, S. Adhesion Property and Morphology of Styrene Triblock/Diblock Copolymer Blends. *J. Appl. Polym. Sci.* **2010**, *118*, 1766−1773.
(26) Sasaki, M.; Fujita, K.; Adachi, M.; Fujii, S.; Nakamura, Y.; Urahama, Y. The Effects of Tackifier on Phase Structure and Peel Adhesion of a Triblock Copolymer Pressure-Sensitive Adhesive. *Int. J. Adhes. Adhes.* **2008**, *28*, 372−381.
(27) Nakamura, Y.; Adachi, M.; Ito, K.; Kato, Y.; Fujii, S.; Sasaki, M.; Urahama, Y.; Sakurai, S. Effects of Compatibility between Tackifier and Polymer on Adhesion Property and Phase Structure: Tackifier-Added Polystyrene-Based Triblock/Diblock Copolymer Blend System. *J. Appl. Polym. Sci.* **2011**, *120*, 2251−2260.
(28) Nakamura, Y.; Sakai, Y.; Imamura, K.; Ito, K.; Fujii, S.; Urahama, Y. Effects of the Compatibility of a Polyacrylic Block Copolymer/Tackifier Blend on the Phase Structure and Tack of a Pressure-Sensitive Adhesive. *J. Appl. Polym. Sci.* **2012**, *123*, 2883−2893.
(29) Brandrup, J.; Immergut, E. H. *Polymer Handbook*; 3rd ed.; John Wiley & Sons. Inc.: 1989, Vol. *82*.
(30) Brandrup, J.; Immergut, E. H. *Polymer Handbook*; 3rd ed.; John Wiley & Sons. Inc.: 1989, Vol. *7*.
(31) Watanabe, H. Slow Dielectric Relaxation of a Styrene-Isoprene-Styrene Triblock Copolymer with Dipole Inversion in the Middle Block: A Challenge to a Loop/Bridge Problem. *Macromolecules* **1995**, *28*, 5006−5011.
(32) Watanabe, H.; Sato, T.; Osaki, K. Concentration Dependence of Loop Fraction in Styrene-Isoprene-Styrene Triblock Copolymer Solutions and Corresponding Changes in Equilibrium Elasticity. *Macromolecules* **2000**, *33*, 2545−2550.
(33) Watanabe, H.; Tan, H. Dielectric Investigation of Bridge Fraction in Triblock/Diblock Mixed Lamella. *Macromolecules* **2004**, *37*, 5118−5122.
(34) Watanabe, H.; Matsumiya, Y.; Sawada, T.; Iwamoto, T. Rheological and Dielectric Behavior of Dipole-Inverted (SIS)p-Type Multiblock Copolymers: Estimates of Bridge/Loop Fractions for Respective I Blocks and Effect of Loops on High Extensibility of Bridges. *Macromolecules* **2007**, *40*, 6885−6897.
(35) Sakurai, S.; Kawada, H.; Hashimoto, T.; Fetters, L. J. Thermoreversible Morphology Transition between Spherical and Cylindrical Microdomains of Block Copolymers. *Macromolecules* **1993**, *26*, 5796−5802.
(36) Tomita, S.; Shimizu, N.; Igarashi, N.; Takagi, H.; Sasaki, S.; Sakurai, S. Coalescence of non-equilibrium spheres through thermal-annealing in an SEBS triblock copolymer film under a uniaxially stretched state. *Polym. J.* **2017**, *49*, 519−526.
(37) Kota, T.; Imaizumi, K.; Sasaki, S.; Sakurai, S. Spontaneous Enhancement of Packing Regularity of Spherical Microdomains in the Body-Centered Cubic Lattice upon Uniaxial Stretching of Elastomeric Triblock Copolymers. *Polymer* **2011**, *3*, 36−50.
(38) Uozumi, M.; Matsushita, T.; Sakamoto, N.; Yamazaki, T.; Imaizumi, K.; Li, L.; Urushihara, Y.; Kuwamoto, S.; Masunaga, H.; Sasaki, S.; Sakurai, S. Changes in Microphase-Separated Structures and Properties of an Elastomeric Block Copolymer Film Upon Uniaxial Stretching as Analyzed by Conducting Simultaneous Measurements of Two-Dimensional Small-Angle X-ray Scattering with Stress-Strain Tests. *J. Soc. Rheol., Jpn.* **2015**, *43*, 77−83.
(39) Ehrburger-Dolle, F.; Morfin, I.; Bley, F.; Livet, F.; Heinrich, G.; Piché, L.; Sutton, M. Experimental Clues of Soft Glassy Rheology in Strained Filled Elastomers. *J. Polym. Sci., Part B: Polym. Phys.* **2014**, *52*, 647−656.
(40) Tada, T.; Urayama, K.; Mabuchi, T.; Muraoka, K.; Takigawa, T. Nonlinear Stress Relaxation of Carbon Black-Filled Rubber Vulcanizates under Various Types of Deformation. *J. Polym. Sci., Part B: Polym. Phys.* **2010**, *48*, 1380−1387.
(41) Ferry, J. D. Cross-Linked Polymers and Composites Systems. In *Viscoelastic Properties of Polymers*; 3rd ed. Wiley: New York, 1980, Chapter 14, p.404−436.
(42) Curro, J. G.; Pincus, P. A Theoretical Basis for Viscoelastic Relaxation of Elastomers in the Long-Time Limit. *Macromolecules* **1983**, *16*, 559−562.
(43) Joubert, C.; Michel, A.; Choplin, L.; Cassagnau, P. Influence of the Crosslink Network Structure on Stress-Relaxation Behavior: Viscoelastic Modeling of the Compression Set Experiment. *J. Polym. Sci., Part B: Polym. Phys.* **2003**, *41*, 1779−1790.
(44) Ferry, J. D. *Viscoelastic Properties of Polymers*; (Third Edition). John Wiley & Sons: New York, 1980, p.81.
(45) Fujino, K.; Horino, T.; Miyamoto, K.; Kawai, H. Tensile Stress Relaxation Behavior of Partly to Completely Acetylated Polyvinyl Alcohol Polymers. *J. Colloid Sci.* **1961**, *16*, 411−430.
(46) Saunders, P. R.; Stern, D. M.; Kurath, S. F.; Sakoonkim, C.; Ferry, J. D. Dynamic Mechanical Properties of Concentrated Solutions of Poly-*n*-Butyl Methacrylate in Diethyl Phthalate. *J. Colloid Sci.* **1959**, *14*, 222−238.
(47) Doi, T.; Takagi, H.; Shimizu, N.; Igarashi, N.; Sakurai, S. Effects of Drying Temperature in Solution Coating Process on Microphase-Separated Structures in Coated Layers of Pressure-Sensitive Adhesive Composed of Di- and Triblock Copolymer Blends as Revealed by Small-Angle X-Ray Scattering. *Polymer* **2019**, *170*, 211−221.
(48) Doi, T.; Takagi, H.; Shimizu, N.; Igarashi, N.; Sakurai, S. Effects of Drying Temperature in Solution Coating Process on the Structural Changes upon Uniaxial Stretching of Sphere-Forming Block Copolymer Films. *Polym. J.* **2020**, *52*, 421−433.
(49) Ohnogi, H.; Sasaki, S.; Sakurai, S. Evaluation of Grain Size by Small-Angle X-Ray Scattering for a Block Copolymer Film in which Cylindrical Microdomains are Perpendicularly Oriented. *Macromol. Symp.* **2016**, *366*, 35−41.

https://doi.org/10.1021/acsomega.1c01367
ACS Omega 2021, 6, 17299−17313